

Application of belief functions to medical image segmentation: A review

Ling Huang^{a,b}, Su Ruan^b

^a*Heudiasyc, CNRS, Université de technologie de Compiègne, France*

^b*Quantif, LITIS, University of Rouen Normandy, France*

Abstract

Belief function theory, a formal framework for uncertainty analysis and multiple evidence fusion, has made significant contributions in the medical domain, especially since the development of deep learning. Medical image segmentation with belief function theory has shown significant benefits in clinical diagnosis and medical image research. In this paper, we provide a review of medical image segmentation methods using belief function theory. We classify the methods according to the fusion step and explain how information with uncertainty or imprecision is modeled and fused with belief function theory. In addition, we discuss the challenges and limitations of present belief function-based medical image segmentation and propose orientations for future research. Future research could investigate both belief function theory and deep learning to achieve more promising and reliable segmentation results.

Keywords: Medical image segmentation, Information fusion, Evidence fusion, Belief function theory, Dempster-Shafer theory, Evidence theory, Uncertainty quantification, Deep learning

1. Introduction

The precise delineation of the target lesion on the medical image is essential for optimizing disease treatment. In clinical routine, this segmentation is performed manually by physicians. It is time-consuming with 3D images and can vary greatly from one expert to another. Thus, it is necessary to develop automatic segmentation algorithms for helping physicians in radiotherapy planning. Traditional image segmentation methods use the information provided by the image itself, such as threshold (Batenburg and Sijbers, 2009),

edge detection (Kimmel, 2003), histograms (Ohlander et al., 1978), region growing (Nock and Nielsen, 2004), graph partitioning (Grady and Schwartz, 2006; Onoma et al., 2014), and clustering (Salvador and Chan, 2004), or use machine learning-based supervised methods such as support vector machine (SVM) (Suykens and Vandewalle, 1999; Ruan et al., 2007), random forest (RF) (Strobl et al., 2007) and logistic regression (LR) (Kleinbaum and Hedeker, 1996). Those methods have attracted great interest, but their results cannot meet the expectation of clinical segmentation accuracy because only low-level features, such as pixel, texture and contrast, are considered. High segmentation performance requires not only the analysis of low-level features but also the analysis of high-level semantic features.

Deep learning, a sub-field of machine learning concerned with neural networks, is inspired by the structure and the function of human brain and has achieved significant achievements in computer vision tasks (Krizhevsky et al., 2012; Bai et al., 2018; Huang et al., 2019), as well as in medical image segmentation domain (Ciresan et al., 2012; Seyedhosseini et al., 2013; Hariharan et al., 2015; Long et al., 2015; Ronneberger et al., 2015). Ciresan et al. (2012) proposed a pixel-level classification network for electron microscopy (EM) image segmentation. This network won the competition of EM segmentation challenge at ISBI 2012 by a large margin. Seyedhosseini et al. (2013) proposed a multiresolution contextual model, called cascaded hierarchical model (CHM). Hariharan et al. (2015) used hyper columns as pixel descriptors to make the best use of semantic contextual and allow precise location. Fully connected network (FCN) (Long et al., 2015), a milestone of medical image segmentation, shows that a fully convolutional neural network can be trained end-to-end for pixel-level prediction. UNet (Ronneberger et al., 2015), a successful modification and extension of FCN, has become the most popular network for medical image segmentation in recent years. Based on UNet, abundant extension and optimization work has been done, such as 3D UNet (Çiçek et al., 2016), Res-UNet (Xiao et al., 2018), Dense-UNet (Guan et al., 2019), MultiResUNet (Ibtehaz and Rahman, 2020), Deep3D-UNet (Zhu et al., 2018), etc. Deep learning-based segmentation methods show good performance under the assumption that much high-quality training data and precise annotations are available, while acquiring a large amount of labeled training data in the medical domain is challenging, especially for medical segmentation tasks. Thus many researchers pay attention to developing deep learning-based segmentation methods that use only partially labeled or unlabelled data. These methods can be classified into three cat-

egories according to their training methods: self-training-based methods (Li et al., 2019), adversarial training-based methods (Goodfellow et al., 2014), and co-training-based methods (Peng et al., 2020).

The medical domain has witnessed great success thanks to the strong learning ability of deep learning. At the same time, the limitations of medical imaging technology still result in the low resolution and high uncertainty of medical images (noise, fuzzy boundary, etc), which are always the obstacles between experimental performance and clinical application. Besides deep learning, another direction of research has been to model uncertainty in image processing and evidence fusion. Among these approaches, we are interested in belief function theory (BFT) in this paper. BFT (Dempster, 1967; Shafer, 1976), also be known as Dempster-Shafer theory (DST) or Evidence theory, is a theory for information modeling, evidence fusion and decision reasoning with uncertain or imprecise information. The great expressivity of BFT allows us to represent evidence more reliably and cautiously than probabilistic approaches. Researchers from the medical image community have actively involved in the research of BFT in handling uncertainty information modeling and fusion for different medical tasks, such as disease classification (Lian et al., 2016; Huang et al., 2021d), lesion segmentation (Huang et al., 2021c; Lian et al., 2018b), uncertainty quantification (Ghesu et al., 2021; Huang et al., 2021c), information fusion (Velikova et al., 2012), etc.

In this paper, we provide an overview of BFT-based medical image segmentation methods, with a main focus on information modeling and multiple evidence fusion. We hope this review will raise the community’s awareness of the existing solutions for information modeling and fusion of medical image segmentation and further inspire researchers to explore the possibility of taking the benefit of both BFT and deep learning to make automatic segmentation methods interpretable and reliable.

We organize this paper as follows: Section 2 introduces the fundamentals of BFT. Section 3 gives an overall perspective of BFT-based medical image segmentation. Sections 4 and 5 present the BFT-based medical image segmentation with, respectively, single and multiple classifiers or clustering algorithms. Section 6 concludes this review.

Search criterion. To identify related contributions, we mainly retrieved papers containing “medical image segmentation” and “belief function theor” or “Dempster-Shafer theory” or “evidence theory” in the title or abstract from IEEE, Springer, PubMed, Google Scholar, and ScienceDirect. Additionally, conference proceedings for MICCAI, ISBI were searched based on

the titles of papers. Papers that do not primarily focus on medical image segmentation problems were excluded.

2. Fundamentals of belief function theory

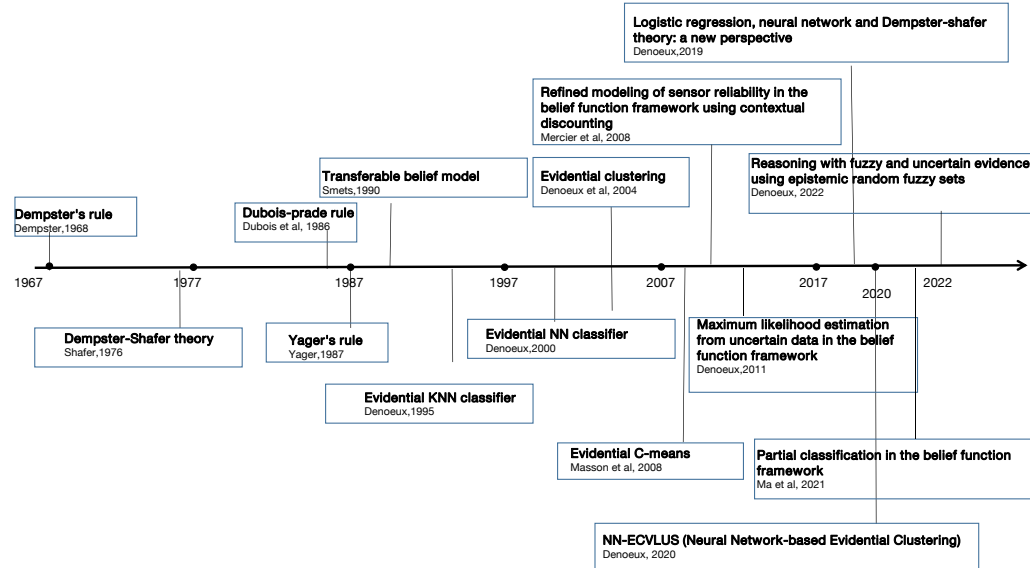


Figure 1: Partial history of the belief function theory.

BFT is a generalization of Bayesian theory, but it is more flexible than the Bayesian approach and more suitable for weaker conditions (Sun and Wang, 2018), i.e., imperfect (uncertain, imprecise, partial) information. In the past decades, BFT has generated considerable interests and has had a great success in diverse fields, including uncertain reasoning (Smets, 1990; Yager, 1987; Dubois and Prade, 1988; Denœux, 2008), classification (Denœux, 1995, 2000) and clustering (Denœux and Masson, 2004; Masson and Denœux, 2009), etc. Figure 1 shows a view of the development process of BFT with a selection of landmark papers. It was first originated by Dempster (1967) in the context of statistic inference and was formalized by Shafer (1976) as a theory of evidence. Dubois and Prade (2012) proposed an approach to computerized processing of uncertainty. Yager (1987) proposed a new combination rule of the belief function framework. In 1990, BFT was further popularized and developed by Smets (1990) as the 'Transferable Belief Model' with pignistic transformation for decision making. Since then, booming developments

have been made thanks to the flexible computation of BFT with pignistic transformation. Denœux (1995) proposed a distance-based K-NN classifier for classification task. Denœux (2000) applied the distance-based evidential classifier within the neural network and trained the model end-to-end. Denœux and Masson (2004) proposed an evidential clustering algorithm that extends the notion of fuzzy partition with mass functions and applies uncertain reasoning with the defining of credal partition. Masson and Denœux (2008) introduced Evidential C-Means in the theoretical framework of belief functions. Mercier et al. (2008) proposed to refine sensor reliability in the belief function framework using contextual discounting. Denœux (2011) introduced a maximum likelihood estimation method from uncertain data in the belief function framework. Denœux et al. (2019) discussed the relationship between Logistic regression, neural network and Dempster-Shafer theory and offered a new perspective for future research. Denœux (2021a) first applied the evidential clustering algorithm within the neural network. Ma and Denœux (2021) proposed partial classification in the belief function framework. Denœux (2022) proposed reasoning with fuzzy and uncertain evidence using epistemic random fuzzy sets.

We first introduce the basic notions of BFT in Section 2.1, which includes evidence representation (mass functions, belief, and plausibility functions). Second, we introduce Dempster’s combination rule to explain the operations of multiple sources of evidence in Section 2.2. Third, we introduce discounting operation for unreliable sources in Section 2.3. Fourth, we introduce some decision-making methods in Section 2.4. The applications of BFT to classification and clustering tasks are introduced in Sections 2.5 and 2.6. Finally, We introduce some basic belief assignment methods used for medical image segmentation in Section 2.7.

2.1. Representation of evidence

Let $\Omega = \{\omega_1, \omega_2, \dots, \omega_C\}$ be a finite set of all possible hypotheses about some problem, called a frame of discernment. Evidence about a variable ω taking values in Ω can be represented by mass function m , also called basic belief assignment (BBA), from the power set 2^Ω to $[0, 1]$, such that

$$\sum_{A \subseteq \Omega} m(A) = 1, \quad (1a)$$

$$m(\emptyset) = 0. \quad (1b)$$

Each subset $A \subseteq \Omega$ and $m(A)$ is called a focal set of m . The total ignorance of the problem can be represented as $m(\Omega)$. If all focal sets are singletons, then m is said to be Bayesian, it is equivalent to a probability distribution. The information provided by a mass function m can be represented by a belief function Bel or a plausibility function Pl from 2^Ω to $[0, 1]$, respectively, as

$$Bel(A) = \sum_{B \subseteq A} m(B) \quad (2)$$

and

$$Pl(A) = \sum_{B \cap A \neq \emptyset} m(B) = 1 - Bel(\bar{A}), \quad (3)$$

for all $A \subseteq \Omega$. The quantity $Bel(A)$ can be interpreted as a degree of support to A , while $Pl(A)$ can be interpreted as a measure of lack of support given to the complement of A (or we can say $Pl(A)$ represents the belief that might be committed to A). Figure 2 shows the difference between the probability model and the BF model applied to a three class classification or clustering task. Comparing with the probability-based model, the BF-based model shows advantages in uncertainty quantification by assigning the uncertainty or ignorance into focal sets.

2.2. Dempster's rule

In BFT, the belief about a certain item is elaborated by aggregating different belief functions over the same frame of discernment. Given two mass functions m_1 and m_2 derived from two independent items of evidence, the final belief that supports A can be obtained by combining m_1 and m_2 with Dempster's rule (Shafer, 1976), which is defined as

$$(m_1 \oplus m_2)(A) = \frac{1}{1 - \kappa} \sum_{B \cap D = A} m_1(B)m_2(D), \quad (4)$$

for all $A \subseteq \Omega$, $A \neq \emptyset$, and $(m_1 \oplus m_2)(\emptyset) = 0$. The coefficient κ is the degree of conflict between m_1 and m_2 , it is defined as

$$\kappa = \sum_{B \cap D = \emptyset} m_1(B)m_2(D). \quad (5)$$

Table 1 shows an example of two source evidence fusion by using Dempster's rule for $A = \{a\}, \{b\}$ and $\{a, b\}$. The degree of conflict is $\kappa =$

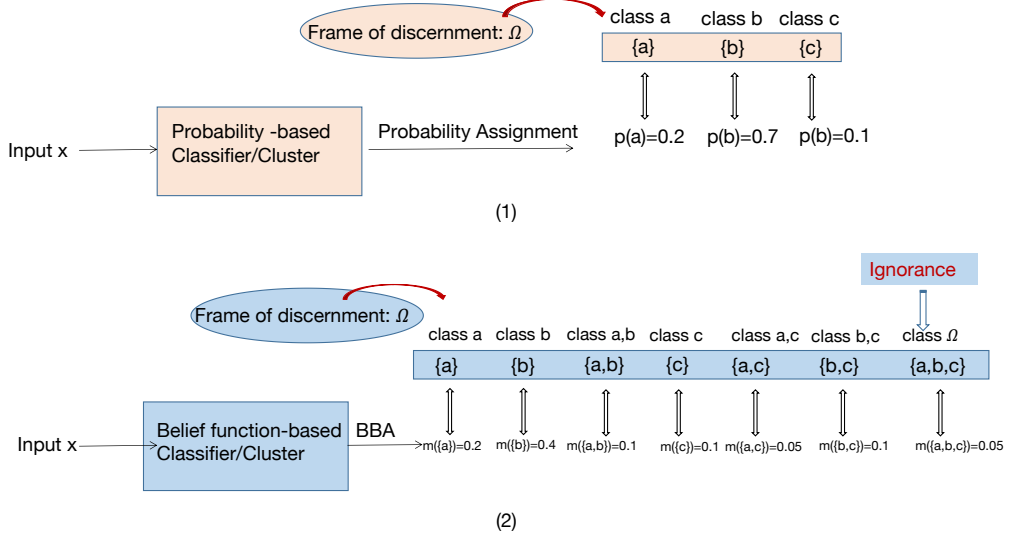


Figure 2: An example of three class assignments: (1) Probabilistic model and (2) BF model. Different from probabilistic model, BF model can quantify uncertainty and assign it into the focal set $\{a, b\}$, $\{a, c\}$, $\{b, c\}$ and $\{a, b, c\}$ to represent its uncertainty or ignorance.

Table 1: Example of Dempster's rule for evidence fusion

$m_1 \backslash m_2$	$\{a\}, 0.2$	$\{b\}, 0.7$	$\{a, b\}, 0.1$
$\{a\}, 0.4$	$\{a\}, 0.08$	$\emptyset, 0.28$	$\{a\}, 0.04$
$\{b\}, 0.1$	$\emptyset, 0.02$	$\{b\}, 0.07$	$\{b\}, 0.01$
$\{a, b\}, 0.5$	$\{a\}, 0.1$	$\{b\}, 0.35$	$\{a, b\}, 0.05$

$0.28 + 0.02 = 0.3$. The combined mass function is

$$(m_1 \oplus m_2)(\{a\}) = (0.08 + 0.1 + 0.04)/(1 - 0.3) = 0.22/0.7 = 0.314,$$

$$(m_1 \oplus m_2)(\{b\}) = (0.07 + 0.35 + 0.01)/(1 - 0.3) = 0.43/0.7 = 0.614,$$

$$(m_1 \oplus m_2)(\{a, b\}) = 0.05/0.7 = 0.072.$$

2.3. Discounting

In (5), if m_1 and m_2 are logically contradictory and, consequently, then we can not use Dempster's rule to combine the two evidence. Discounting strategies thus can be used to combine evidence under high contradiction

(Shafer, 1976; Mercier et al., 2008; Denœux et al., 2019). Let m be a mass function on Ω and ξ a coefficient in $[0, 1]$. The *discounting* operation (Shafer, 1976) with discount rate ξ transforms m into a weaker, less informative mass function defined as follows:

$$\xi m(A) = (1 - \xi)m(A), \quad \forall A \subset \Omega, \quad (6a)$$

$$\xi m(\Omega) = (1 - \xi)m(\Omega) + \xi, \quad (6b)$$

coefficient $1 - \xi$ represent the degree of belief that the source m is reliable. In medical domain, the discounting function is widely used in multi-modality evidence fusion by taking source information reliability into account and discounts their outputs using these precalculated reliability factors.

2.4. Decision-making

After combining all the available evidence in the form of a mass function, it is necessary to decide the belief to be assigned into focal sets. In this section, we introduce some classical decision-making methods.

2.4.1. Upper and lower expected utilities

Let u be a utility function. The lower and upper expectations of u with respect to m are defined, respectively, as the averages of the minima and the maxima of u within each focal set of m :

$$\underline{E}_m(u) = \sum_{A \subseteq \Omega} m(A) \min_{\omega \in A} u(\omega), \quad (7a)$$

$$\overline{E}_m(u) = \sum_{A \subseteq \Omega} m(A) \max_{\omega \in A} u(\omega). \quad (7b)$$

When m is Bayesian, $\underline{E}_m(u) = \overline{E}_m(u)$. If m is logical with focal set A , then $\underline{E}_m(u)$ and $\overline{E}_m(u)$ are, respectively, the belief and plausibility functions as we mentioned in Section 2.1. Both lower or upper expectations can be chosen for the final decision according to the given task.

2.4.2. Generalized Hurwicz criterion

Since the upper and lower expected utilities can be obtained, the Hurwicz criterion (Hurwicz, 1951) can be generalized by defining the expectation of m

$$E_{m,\varsigma}(u) = \sum_{A \subseteq \Omega} m(A) \left(\varsigma \min_{\omega \in A} u(\omega) + (1 - \varsigma) \max_{\omega \in A} u(\omega) \right) = \varsigma \underline{E}_m(u) + (1 - \varsigma) \overline{E}_m(u), \quad (8)$$

where $\varsigma \in [0, 1]$ is a parameter called pessimism index.

2.4.3. Pignistic criterion

Smets (1990) proposed a pignistic transformation that each mass of belief is distributed equally among the elements for all, which is defined as

$$BetP(\omega) = \sum_{\omega \in A} \frac{m(A)}{|A|}, \quad \forall \omega \in \Omega, \quad (9)$$

where $|A|$ denotes the cardinality of $A \subseteq \Omega$.

Beside on the above methods, there are various decision-making methods that proposed for BFT, such as Generalized OWA criterion (Yager, 1992), Generalized minimax regret(Yager, 2004), Jaffray's and related axioms (Jaffray, 1989), etc. More details about decision-making with BFT can be found in the review paper (Denœux, 2019a).

2.5. Application to classification

Based on the basic BFT, further improvements and applications have been made by researchers in this domain. We introduce the BFT-based classification work in this section.

A classification problem is given a learning set $Z = \{(x_1, y_1), \dots, (x_n, y_n)\}$, to predict the class label of a new instance x , where x_i is the training sample, and y_i is the correspond label. There are two main kinds of evidential classifiers. One is the likelihood-based classifier, such as Shafer's model (Shafer, 1976) and Appriou's model (Appriou, 1999, 2005). The other is distance-based classifier, such as evidential K-NN (Denœux, 1995), evidential neural network classifier (Denœux, 2000) and Radial basis function network (Denœux, 2019a).

2.5.1. The likelihood-based classifier

Shafer's model. Shafer (1976) proposed a likelihood-based evidential model to calculate mass functions. Assuming that conditional density functions $f(x | \omega_c)$ are known, then the conditional likelihood associated with the pattern X is defined by $\ell(\omega_c | x) = f(x | \omega_c)$. The mass functions are defined according to the knowledge of all hypotheses $\omega_1, \dots, \omega_C$. Firstly, the plausibility of a simple hypothesis ω_c is proportional to its likelihood. The plausibility is thus given by

$$Pl(\{\omega_c\}) = \hbar \cdot \ell(\omega_c | x), \quad \forall \omega_c \in \Omega, \quad (10)$$

where \hbar is a normalization factor with $\hbar = 1 \max_{\omega \in \Omega} \ell(\omega | x)$. The plausibility of a set A is thus given by

$$Pl(A) = \hbar \cdot \max_{\omega_c \in A} \ell(\omega_c | x). \quad (11)$$

Appriou's model. As Shafer's one, Appriou (1999, 2005) proposed two likelihood based models to calculate mass functions with the frame of discernment $\Omega = \{\omega_c, \neg\omega_c\}$. For the first model, the mass functions are defined by

$$m(\{\omega_c\}) = 0, \quad (12a)$$

$$m(\{\neg\omega_c\}) = \alpha_c (1 - \hbar \cdot \ell(\omega_c | x)), \quad (12b)$$

$$m(\Omega) = 1 - \alpha_c (1 - \hbar \cdot \ell(\omega_c | x)), \quad (12c)$$

where α_c is a reliability factor depending on the hypothesis ω_c and on the source information. The second model is defined as

$$m(\{\omega_c\}) = \alpha_c \cdot \hbar \cdot \ell(\omega_c | x) / (1 + \hbar \cdot \ell(\omega_c | x)), \quad (13a)$$

$$m(\{\neg\omega_c\}) = \alpha_c / (1 + \hbar \cdot \ell(\omega_c | x)), \quad (13b)$$

$$m(\Omega) = 1 - \alpha_c. \quad (13c)$$

2.5.2. The distance-based classifier

Evidential K-NN (EKNN) rule. Denœux (1995) proposed a distance-based K-NN classifier for classification task. Let $N_K(x)$ denote the set of the K nearest neighbors of x in learning set Z . Each $x_i \in N_K(x)$ is considered as a piece of evidence regarding the class label of x . The strength of an evidence decreases with the distance between x and x_i . The evidence of (x_i, y_i) support class c is represented by

$$m_i(\{\omega_c\}) = \varphi_c(d_i) y_{ic}, \quad 1 \leq c \leq C, \quad (14a)$$

$$m_i(\Omega) = 1 - \varphi_c(d_i), \quad (14b)$$

where d_i is the distance between x and x_i , which can be Euclidean or other distance function; and $y_{ic} = 1$ if $y_i = \omega_c$ and $y_{ic} = 0$ otherwise. The parameter φ_c is a decreasing function with

$$\varphi_c(d) = \alpha \exp(-\gamma d^2), \quad (15)$$

where α and γ are two tuning parameters. The evidence of the K nearest neighbors of x is fused by Dempster's rule:

$$m = \bigoplus_{x_i \in N_K(x)} m_i. \quad (16)$$

The final decision is made according to maximum plausibility. The detailed optimization of these parameters is described in (Zouhal and Denœux, 1998). Based on the first work, Denœux et al. (2019) propose contextual discounting evidential K-NN with partially supervised learning to address the annotation limitation problem.

Evidential neural network (ENN). The success of machine learning encouraged the exploration of applying belief function theory with learning methods. Denœux (2000) proposed an ENN classifier, in which mass functions are computed based on distances to prototypes. The basic idea is to consider each prototype as a piece of evidence, which is discounted based on its distance to the input vector. The evidence from different prototypes is then pooled by Dempster's rule (4) and (5). We provide a brief introduction to the ENN classifier in this section.

The ENN classifier is composed on an input layer of H neurons, two hidden layers and an output layer. The first input layer is composed of I units, whose weights vectors are prototypes p_1, \dots, p_I in input space. The activation of unit i in the prototype layer is

$$s_i = \alpha_i \exp(-\gamma_i d_i^2), \quad (17)$$

where $d_i = \|x - p_i\|$ is the Euclidean distance between input vector x and prototype p_i , $\gamma_i > 0$ is a scale parameter, and $\alpha_i \in [0, 1]$ is an additional parameter. The second hidden layer computes mass functions m_i representing the evidence of each prototype p_i , using the following equations:

$$m_i(\{\omega_c\}) = u_{ic} s_i, \quad c = 1, \dots, C \quad (18a)$$

$$m_i(\Omega) = 1 - s_i, \quad (18b)$$

where u_{ic} is the membership degree of prototype i to class ω_c , and $\sum_{c=1}^C u_{ic} = 1$. Mass function m_i can thus be seen as a discounted Bayesian mass function, with discount rate $1 - s_i$; its focal sets are singletons and Ω . The mass assigned to Ω increases with the distance between x and p_i . Finally, the third layer combines the I mass functions m_1, \dots, m_I using Dempster's rule. The output mass function $m = \bigoplus_{i=1}^I m_i$ is a discounted Bayesian mass function that summarizes the evidence of the I prototypes.

Let θ denote the vector of all network parameters, composed of the I prototypes p_i , their parameters γ_i and α_i , and their membership degrees u_{ic} ,

$c = 1, \dots, C$. Those parameters are learnt by minimizing the regularized sum-of-squares loss function

$$L_{SS}(\boldsymbol{\theta}) = \sum_{n=1}^N \sum_{c=1}^C (p_{nc} - y_{nc})^2 + \lambda \sum_{i=1}^I \alpha_i, \quad (19)$$

where p_{nc} is the pignistic probability of class ω_c for instance n , and $y_{nc} = 1$ if the true class of instance n is ω_c , and $y_{nc} = 0$ otherwise. The second term on the right-hand side of (19) is a regularization term, and λ is hyperparameter that can be tuned by cross-validation.

The idea of applying the above model to features extracted by a convolutional neural network (CNN) was first proposed by (Tong et al., 2021). In this approach, the ENN module becomes a “DS layer” that is plugged into the output of a CNN instead of the usual softmax layer. The feature extraction and evidential modules are trained simultaneously. Some similar approach was applied in (Huang et al., 2021c,b, 2022) to medical image segmentation, which will be introduced in Section 4.

Radial basis function (RBF) network. As confirmed in (Huang et al., 2022) that RBF network can be an alternative approach of ENN that based on the aggregation of weights of evidence.

Consider an RBF network with I prototype (hidden) units. The activation of hidden unit i is

$$s_i = \exp(-\gamma_i d_i^2), \quad (20)$$

where, $d_i = \|\mathbf{x} - \mathbf{p}_i\|$ is the Euclidean distance between input vector \mathbf{x} and prototype \mathbf{p}_i , and $\gamma_i > 0$ is a scale parameter. Here we only show an example of binary classification task $C = 2$ and $\Omega = \{\omega_1, \omega_2\}$ (The multi-class example can be found in (Denœux, 2019b)). Let v_i be the weight of the connection between hidden unit i and the output unit, and let $w_i = s_i v_i$ be the product of the output of unit i and weight v_i . The quantities w_i can be interpreted as weights of evidence for class ω_1 or ω_2 , depending on the sign of v_i . If $v_i > 0$, w_i is a weight of evidence for class ω_1 ; if $v_i < 0$, $-w_i$ is a weight of evidence for class ω_2 . To each prototype i can be associated the following simple mass function:

$$m_i = \{\omega_1\}^{w_i^+} \oplus \{\omega_2\}^{w_i^-},$$

where w_i^+ and w_i^- denote, respectively, the positive and negative parts of w_i . Combining the evidence of all prototypes in favor of ω_1 or ω_2 by Dempster’s

rule, we get the mass function

$$m = \bigoplus_{i=1}^I m_i. \quad (21)$$

Mass function m defined by (21) has the following expression:

$$m(\{\omega_1\}) = \frac{[1 - \exp(-w^+)] \exp(-w^-)}{1 - \kappa}, \quad (22a)$$

$$m(\{\omega_2\}) = \frac{[1 - \exp(-w^-)] \exp(-w^+)}{1 - \kappa}, \quad (22b)$$

$$m(\Omega) = \frac{\exp(-w^+ - w^-)}{1 - \kappa} = \frac{\exp(-\sum_{i=1}^I |w_i|)}{1 - \kappa}, \quad (22c)$$

where κ is the degree of conflict between $\{\omega_1\}^{w^+}$ and $\{\omega_2\}^{w^-}$ with

$$\kappa = [1 - \exp(-w^+)] [1 - \exp(-w^-)]. \quad (23)$$

The idea of applying the RBF within convolutional neural network (CNN) was first proposed by (Huang et al., 2022). In this paper, the RBF module becomes a “evidential module” that is plugged into the output of a CNN instead of the usual Softmax layer. The parameters in this classifier can be learned by minimizing a loss function such as, e.g., the regularized cross-entropy loss

$$L_{CE}(\boldsymbol{\theta}) = - \sum_{n=1}^N (y_n \log p_n + (1 - y_n) \log(1 - p_n)) + \lambda \sum_{i=1}^I w_i^2, \quad (24)$$

where p_n is the normalized plausibility of class ω_1 for instance n , and λ is a hyperparameter.

2.6. Application to clustering

In this section, we introduce the BFT-based clustering work. A clustering problem can be described as given a dataset set $Z = \{x_1, \dots, x_n\}$, the goal is to find a algorithm to discover groups in data properly without any label information. What distinguish BFT-based clustering methods from others is the ability to assess the uncertainty in group membership.

Fuzzy C-means (FCM). Considering that there are some BFT-based methods use FCM (Dunn, 1973) for initial clustering, thus we introduce it here to offer a basic view for readers. With FCM, any \mathbf{x} has a set of coefficients giving the degree of being in the k -th cluster $w_k(x)$. The centroid of a cluster is the mean of all points, weighted by their degree of belonging to the cluster,

$$c_k = \frac{\sum_x w_k(x)^m x}{\sum_x w_k(x)^m}, \quad (25)$$

where m is the hyper-parameter that controls how fuzzy the cluster will be. The higher it is, the fuzzier. Given a finite set of data, the FCM algorithm returns a list of cluster centres $P = \{c_1, \dots, c_C\}$ and a partition matrix $W = \omega_{ij}, i = 1, \dots, N, j = 1, \dots, C$,

$$w_{ij} = \frac{1}{\sum_{k=1}^C \left(\frac{\|\mathbf{x}_i - \mathbf{c}_k\|}{\|\mathbf{x}_i - \mathbf{c}_c\|} \right)^{\frac{2}{m-1}}}, \quad (26)$$

where w_{ij} , is the the degree of \mathbf{x}_i belongs to cluster \mathbf{c}_j . The objective function of is defined as

$$\arg \max_P \sum_{i=1}^N \sum_{j=1}^C w_{ij}^m \|\mathbf{x}_i - \mathbf{c}_j\|. \quad (27)$$

Credal partition. In BFT, the uncertainty about the membership of objects to clusters can be represented by the notion of credal partition (Denœux and Masson, 2003, 2004). The credal partition extends the existing concepts of hard, fuzzy (probabilistic), and possibilistic partition by allocating each object a 'mass of belief,' not only to single clusters but also to any subsets of $\Omega = \{\omega_1, \dots, \omega_C\}$. The credal partition allows us to go deeper insight into the data and to improve robustness as well as to address outliers. Table 2 shows an example of credal partition. Assuming there is a collection of five objects for two classes. Mass functions for each source are given in Table 2. They represent different situations: the class of source 1 indicates strong evidence that the class of source 1 does not lie in any focal set; the class of source 2 is completely unknown and the class of source 3 is known with certainty; the cases of sources 4 and 5 correspond to situations of partial knowledge (m_5 is Bayesian). Deriving a credal partition from object data implies determining, one can then assign basic belief to each partition with the given objective functions.

A	$m_1(A)$	$m_2(A)$	$m_3(A)$	$m_4(A)$	$m_5(A)$
$\{\emptyset\}$	1	0	0	0	0
$\{a\}$	0	0	1	0.5	0.6
$\{b\}$	0	0	0	0.3	0.4
$\{a, b\}$	0	1	0	0.2	0

Table 2: Example of credal partition

Evidential C-means (ECM). (Denœux and Masson, 2004) proposed an evidential clustering algorithm. The algorithm extends the notion of fuzzy partition with mass functions and applies uncertain reasoning in the space of all partitions with the defining of credal partition by assigning each object a mass function to all the subsets of the whole frame Ω , not only one focal set. A new clustering method, Evidential C-Means (ECM), was introduced in the theoretical framework of belief functions (Masson and Denœux, 2008). In ECM, a cluster is represented by a prototype p_c . For each non-empty set $A_j \subseteq \Omega$, a prototype \bar{p}_j is defined as the center of mass of the prototypes p_c such that $\omega_c \in A_j$. Then the non-empty focal set is defined as $F = \{A_1, \dots, A_f\} \subseteq 2^\Omega \setminus \{\emptyset\}$. Deriving a credal partition from object data implies determining, for each object x_i , the quantities $m_{ij} = m_i(A_j)$, $A_i \neq \emptyset$, $A_j \subseteq \Omega$. In such a way that m_{ij} is low (resp. high) when the distance between x_i and the focal set \bar{p}_j is high (resp. low). The distance between an object and any nonempty subset of Ω has thus to be defined by

$$d_{ij}^2 = \|x_i - \bar{p}_j\|^2. \quad (28)$$

The ECM thus can be optimized by minimizing the following function

$$J_{ECM}(M, V) = \sum_{i=1}^n \sum_{j=1}^f |A_j|^\alpha m_{ij}^\beta d_{ij}^2 + \sum_{i=1}^n \delta^2 m_{i\emptyset}^\beta, \quad (29)$$

with

$$\sum_{j=1}^f m_{ij} + m_{i\emptyset} = 1, \quad (30)$$

where $|A_j|$ is the cardinal of A_j , m_{ij} is the mass of the object x_i allocated to the credal cluster A_j , $m_{i\emptyset}$ is the mass of the object x_i allocated to the empty set, α controls the specificity of mass functions, β controls the hardness of the

credal partition, δ controls the proportion of outlier data. There are lots of variants clustering algorithms based on ECM. More details about evidential clustering can be found in the review paper (Denœux and Kanjanatarakul, 2016). For example, spatial ECM is a successful extension (Lelandais et al., 2014; Lian et al., 2017b) that takes additional spatial information for clustering and be applied to 3D medical images segmentation tasks, which will be introduced in Section 4.

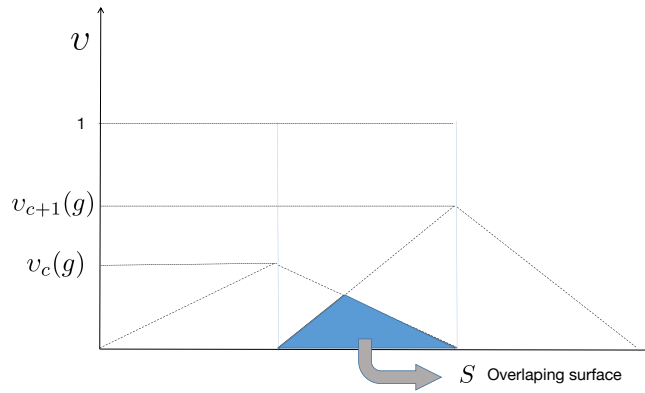


Figure 3: Construction of triangular membership functions and determination of the overlapped surface used for calculating the mass function of double hypothesis.

Zhu's model. (Zhu et al., 2002) proposed a method to determine mass functions using FCM and neighbourhood information. Mass of simple hypothesis $\{\omega_c\}$ is directly obtained from the filtered membership functions $v_c(g)$ of the gray level $g(x, y)$ to cluster c as $m(\{\omega_c\}) = v_c(g)$, indicates that for a given gray level, the piece of evidence of belonging to the cluster c is directly given by its degree of membership to the same cluster. If there is a high ambiguity in assigning a gray level $g(x, y)$ to cluster c or $c + 1$, that is, $|v_c(g) - v_{c+1}(g)| < \varepsilon$, where ε is a thresholding value, then a double hypothesis is formed. The value of the threshold ε is chosen following the applications in question. The authors suggested to fix ε at 0.1. Once the double hypotheses are formed, their associated mass is calculated according to the following formula:

$$m(\{\omega_c, \omega_{c+1}\}) = \frac{S[v_c(g), v_{c+1}(g)]}{2S_{max}}, \quad (31)$$

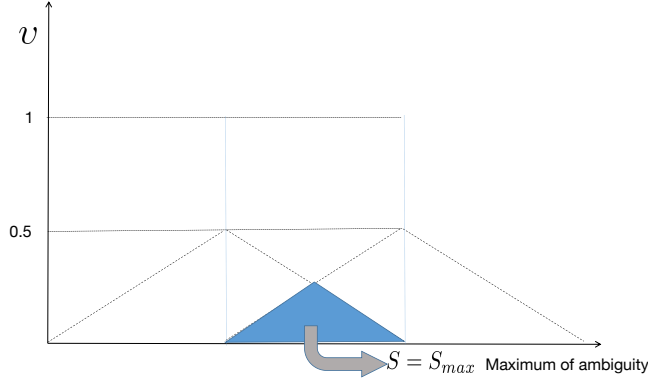


Figure 4: Illustration of the particular triangular membership functions of maximum ambiguity case: $v_c(g) = v_{c+1}(g) = 0.5$.

where S represents a surface of a triangle and S_{max} is the maximum of ambiguity. The surface of such a triangle depends both on the degrees of the membership functions of $g(x, y)$ to clusters c and $c + 1$ and on the conflicts between these membership values. Figure 3 shows how the triangle is constructed and how the mass of double hypotheses $\{\omega_c, \omega_{c+1}\}$ is derived from the surface of the triangle. The vertical axis of Figure 3 represents the membership values. The surface of the two dotted triangles represent two so-called triangular membership functions corresponding to classes c and $c + 1$. The two triangles are isosceles, and have the same length for their bases. The heights of the triangles are equal to $m(\{\omega_c\})$ and $m(\{\omega_{c+1}\})$, respectively. The overlapping surface S of the two triangles represents the membership value to the double hypothesis $\{\omega_c, \omega_{c+1}\}$. Therefore, the mass value attributed to the double hypothesis $\{\omega_c, \omega_{c+1}\}$ can be directly calculated from the surface S . Figure 4 shows the condition of maximum ambiguity case.

Gaussian distribution (GD)-based model. The mass of simple hypotheses $\{\omega_c\}$ can be obtained from the assumption of GD (Chen et al., 2012) according to the information x_i of a pixel from an input image to cluster c as follows:

$$m(\{\omega_c\}) = \frac{1}{\sigma_c \sqrt{2\pi}} \exp \frac{-(x_i - \mu_c)^2}{2\sigma_c^2}, \quad (32)$$

where μ_c and σ_c^2 represent, respectively, the mean and the variance of the cluster c , which can be estimated by

$$\mu_c = \frac{1}{n_c} \sum_{i=1}^{n_c} x_i, \quad (33)$$

$$\sigma_c^2 = \frac{1}{n_c} \sum_{i=1}^{n_c} (x_i - \mu_c)^2, \quad (34)$$

where n_c is the number of pixels in the cluster c . The mass of double hypotheses involves several sets $\{\omega_1, \omega_2, \dots, \omega_T\}$ is determined as

$$m(\{\omega_1, \omega_2, \dots, \omega_T\}) = \frac{1}{\sigma_t \sqrt{2\pi}} \exp \frac{-(x_i - \mu_t)^2}{2\sigma_t^2}, \quad (35)$$

where $\mu_t = \frac{1}{T} \sum_{i=1}^T \mu_i$, $\sigma_t = \max(\sigma_1, \sigma_2, \dots, \sigma_T)$, $2 \leq T \leq C$, C is the number of clusters.

2.6.1. Ratio Membership Value (RMV) transformation

Ghasemi et al. (2012) proposed a ratio membership value transformation method to calculate mass functions. The FCM algorithm was first used to generate membership values (MVs) f_{ω_c} for each pixel. Then the MVs are used to build the mass functions. For this purpose, the three ratios of the available MVs are calculated, corresponding to three situations: no-uncertainty (NU), semi-uncertainty (SU), and perfect-uncertainty (PU). First, PU is a critical situation in which the RMVs are smaller than α , then the mass function is calculated as $m(\{\omega_1\}) = m(\{\omega_2\}) = m(\Omega) = (f_{\omega_1} + f_{\omega_2})/3$. Second, two thresholds α and β with $\alpha = 1.5$ and $\beta = 3$ are selected to control the boundary between SU and PU, and between NU and SU, separately. For example, with

$$f_{\omega_1} = 0.18, f_{\omega_2} = 0.81, RMV = f_{\omega_1}/f_{\omega_2} = 4.5, RMV > \beta,$$

the two membership values fall in the NU category. If

$$f_{\omega_1} = 0.25, f_{\omega_2} = 0.65, RMV = f_{\omega_1}/f_{\omega_2} = 2.6, \alpha < RMV < \beta,$$

the two membership values are in the SU category. The mass functions are calculated using

$$m(\{\omega_1\}) = f_{\omega_1} - \frac{\lambda_{\omega_1, \omega_2}}{2}, \quad (36a)$$

$$m(\{\omega_2\}) = f_{\omega_2} - \frac{\lambda_{\omega_1, \omega_2}}{2}, \quad (36b)$$

$$m(\Omega) = \lambda_{\omega_1, \omega_2}, \quad (36c)$$

where λ is an uncertainty distance value that defined as $\lambda_{\omega_1, \omega_2} = \frac{|f_{\omega_1} - f_{\omega_2}|}{\beta - \alpha}$.

2.6.2. Binary frames of Discernment (BFOD)

Safranek et al. (1990) introduced a BFOD method to transform membership value into mass functions. The BFOD is constructed as $\Omega = \{\omega_c, \neg\omega_c\}$ with a function $cf(\nu)$, $cf(\nu) \in [0, 1]$ that indicates confidence factor. Sigmoid and the one-sided Gaussian function were the most appropriate functions for $cf(\nu)$ reported by the authors. Once a confidence value is obtained, the transformation for mass functions can be accomplished by defining appropriate transfer functions with parameters A and B.

$$m(\{\omega_c\}) = \frac{B}{1 - A} cf(\nu) - \frac{AB}{1 - A}, \quad (37a)$$

$$m(\{\neg\omega_c\}) = \frac{-B}{1 - A} cf(\nu) + B, \quad (37b)$$

$$m(\Omega) = 1 - m(\{\omega_c\}) - m(\{\neg\omega_c\}), \quad (37c)$$

where A and B are user-specific parameters. When the right-hand side goes negative, the left-hand side stays clamped at zero. The parameter A is the confidence-factor axis intercept of the curve that depicts the dependence of $m(\{\omega\})$ on confidence factors, and B is the maximum support value assigned to $m(\{\omega\})$ or $m(\{\neg\omega\})$.

3. Overall perspective of BFT-based medical image segmentation

This section provides an overall perspective of BFT-based medical image segmentation methods. Table 3 is a summary for BFT-based medical image segmentation methods. We sort those methods by publication year and give two attributes. The attribute "Input image type" shows the modality input of medical images. The attribute "Application" indicates segmentation task.

Figure 5 shows the percentage composition of different attributes. Magnetic resonance imaging(MRI, MR images), computed tomography (CT), positron emission tomography (PET), and optical imaging with color are four common modalities for medical image segmentation. As for their applications, brain tissue and brain tumor segmentation account for a large proportion. Interior of the human body segmentation, such as lung, spinal canal, and vertebrae, are also popular tasks for researchers. Researchers also pay attention to skin and cell lesion segmentation with optical imaging with color.

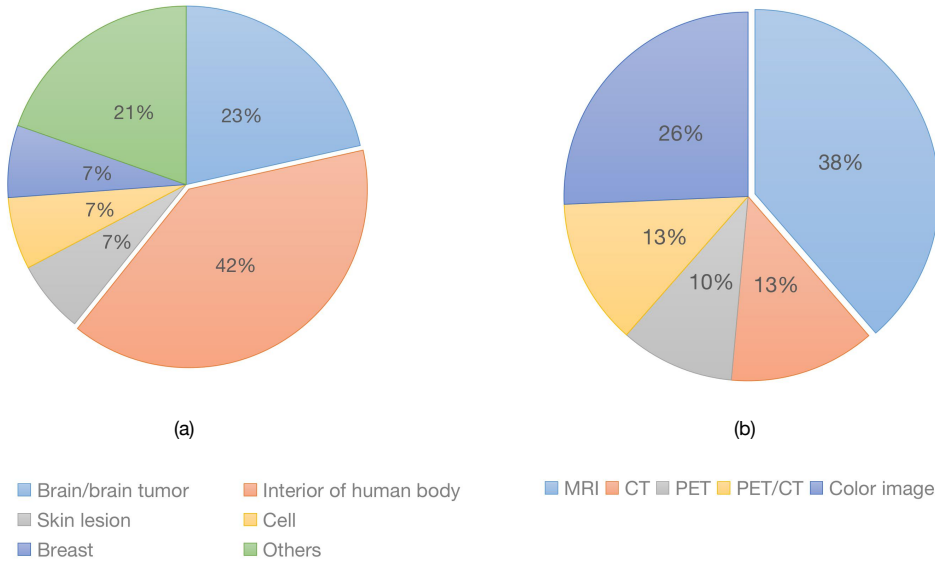


Figure 5: The composition of different attribute partitions: (a)Application, (b) Input image type.

As we motioned in Sections 2.5, 2.6, and 2.7, there are different ways to calculate mass functions. Thus we analyze the mass calculation methods in Table 4. There are some BFT-based segmentation method that use Bayesian instead of mass functions for information fusion (Barhoumi et al., 2007; Ketout et al., 2012; Huang et al., 2021a), or use discounting operation (George et al., 2020) or fuzzy mathematical morphology (Bloch, 2008) to calculate mass function (George et al., 2020), etc. For those methods, we summarized them into the 'Other' class.

Figure 6 gives the summary of BFT-based segmentation methods if multi-modality input or several classifiers/clusters are used. We can see from Figure 6 that 76% of the methods used BFT-based medical images segmentation

with a single classifier or cluster. Among those methods, 18% use single modality input, and 58% use multi-modality input. 24% of BFT-based segmentation methods use several classifiers or clusters. Among those methods, 21% use single modality input, and 3% use multi-modality inputs. We will introduce those methods in detail in Sections 4 and 5. Table 5 shows the detailed fusion level of those methods. Some publications focused on feature-level evidence fusion with a single modality input and a single classifier/cluster. Many publications focused on both feature-level and modality-level evidence fusion with multi-modality input and a single classifier/cluster. Some publications focused on feature-level and classifier-level evidence fusion with a single modality input and several classifiers/clusters. Only a few publications focused on feature-level, modality-level, and classifier-level evidence fusion with multi-modality input and several classifiers/clusters.

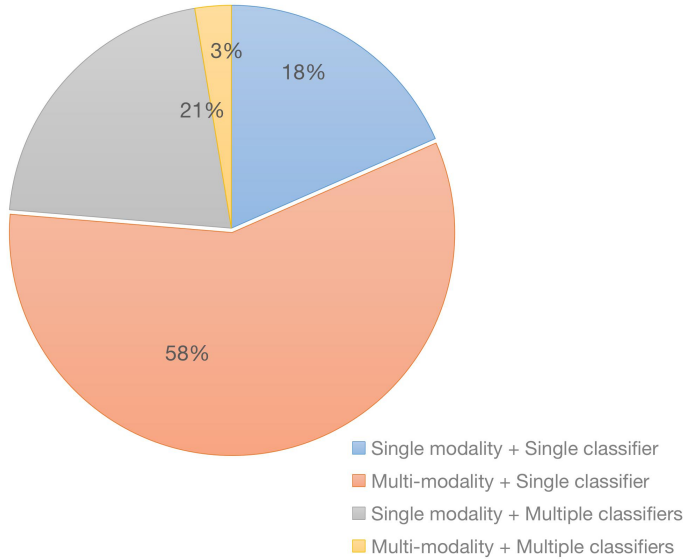


Figure 6: The composition of the number of modality and classifier/cluster.

4. BFT-based medial image segmentation with a single classifier or clusterer

The methods we introduced in this section focus on segmentation with a single classifier or cluster. To make it clear, we classify them into single

Table 3: Summary of the belief function-based approaches for medical image segmentation

Publications	Input image type	Application
Suh et al. (1993)	MR images	cardiac segmentation
Bloch (1996)	MR images	brain tissue segmentation
Vannoorenbergh et al. (1999)	optical imaging with color	skin cancer segmentation
Gautier et al. (2000)	MR images	lumbar sprain segmentation
Gerig et al. (2000)	MR images	brain tissue segmentation
Zhu et al. (2002)	MR images	brain tissue segmentation
Capelle et al. (2002)	MR images	brain tumor segmentation
Taleb-Ahmed and Gautier (2002)	MR images	vertebrae segmentation
Capelle et al. (2004)	MR images	brain tumor segmentation
Vauclin et al. (2005)	CT	lung, spinal canal segmentation
Vannoorenbergh and Flouzat (2006)	CT	thoracic segmentation
Barhoumi et al. (2007)	optical imaging with color	skin lesion malignancy tracking
Bloch (2008)	MR images	brain tissue segmentation
Chaabane et al. (2009)	optical imaging with color	cell lesion segmentation
Chaabane et al. (2011)	optical imaging with color	cell segmentation
Guan et al. (2011)	MR images	brain tissue segmentation
Ketout et al. (2012)	optical imaging with color	endocardial contour detection
Ghasemi et al. (2012)	MR images	brain tissue segmentation
Harrabi and Braiek (2012)	optical imaging with color	breast cancer segmentation
Lelandais et al. (2012)	PET	tumor segmentation
Derraz et al. (2013a)	optical imaging with color	cell segmentation
Derraz et al. (2013b)	optical imaging with color	retinopathy segmentation
Wang et al. (2013)	MR images	cerebra infarction
Ghasemi et al. (2013)	MR images	brain tumor segmentation
Lelandais et al. (2014)	PET-FDG	tumor segmentation
Makni et al. (2014)	MR images	prostate zonal anatomy
Derraz et al. (2015)	PET/CT	lung tumor segmentation
Trabelsi et al. (2015)	optical imaging with color	skin lesion segmentation
Xiao et al. (2017)	CT	vascular segmentation
Lian et al. (2017a)	FDG-PET/CT	lung tumor segmentation
Lian et al. (2017c)	FDG-PET	lung tumor segmentation
Lian et al. (2018a)	FDG-PET/CT	lung cancer segmentation
Lajili et al. (2018)	CT	breast segmentation
Lian et al. (2017b)	PET	lung tumor segmentation
Wen et al. (2018)	MR images	brain tissue segmentation
Tavakoli and Ghasemi (2018)	MR images	brain tissue segmentation
Lima and Islam (2019)	MR images	brain tissue segmentation
Lian et al. (2018b)	PET/CT	lung tumor segmentation
George et al. (2020)	optical imaging with color	breast cancer segmentation
Huang et al. (2021c)	MR images	brain tumor segmentation
Huang et al. (2021a)	PET-CT	lymphoma segmentation
Huang et al. (2021b)	PET-CT	lymphoma segmentation
Huang et al. (2022)	PET-CT	lymphoma segmentation

Table 4: Mass function analysis for belief function-based approaches for medical image segmentation

Publications	Methods to calculate mass functions									
	EKNN	ENN	RBF	ECM	BFOD	RMV	Shafer's model	Appriou's model	Zhu's model	GD-based model
Capelle et al. (2002)	✓									
Vannoorenberghe and Flouzat (2006)	✓									
Capelle et al. (2004)	✓						✓	✓		
Huang et al. (2021c)			✓							
Huang et al. (2021b)			✓							
Huang et al. (2022)			✓	✓						
Lelandais et al. (2014)				✓						
Makni et al. (2014)				✓						
Lian et al. (2017a)				✓						
Lian et al. (2017c)				✓						
Lian et al. (2018a)				✓						
Lian et al. (2017b)				✓						
Lian et al. (2018b)				✓						
Gerig et al. (2000)					✓					
Ghasemi et al. (2012)						✓				
Ghasemi et al. (2013)						✓				
Tavakoli and Ghasemi (2018)						✓				
Lima and Islam (2019)						✓				
Suh et al. (1993)							✓			
Vauclin et al. (2005)							✓			
Chaabane et al. (2009)								✓		
Derraz et al. (2013a)								✓		
Derraz et al. (2013b)								✓		
Derraz et al. (2015)								✓		
Zhu et al. (2002)									✓	
Chaabane et al. (2011)								✓		
Guan et al. (2011)								✓		
Wang et al. (2013)								✓		
Wen et al. (2018)								✓		
Vannoorenberghe et al. (1999)									✓	✓
Harrabi and Braiek (2012)									✓	
Xiao et al. (2017)									✓	
Bloch (1996)										✓
Taleb-Ahmed and Gautier (2002)										✓
Gautier et al. (2000)										✓
Barhoumi et al. (2007)										✓
Bloch (2008)										✓
Ketout et al. (2012)										✓
Lelandais et al. (2012)										✓
Trabelsi et al. (2015)										✓
Lajili et al. (2018)										✓
George et al. (2020)										✓
Huang et al. (2021a)										✓

Table 5: Fusion analysis for the belief function-based approaches for medical image segmentation

Publications	Methods of fusion		
	Feature-level	Modality-level	Classifier/Cluster-level
Suh et al. (1993)	✓		
Gerig et al. (2000)	✓		
Vauclin et al. (2005)	✓		
Vannoorenberghe and Flouzat (2006)	✓		
Derraz et al. (2013a)	✓		
Derraz et al. (2013b)	✓		
Lian et al. (2017b)	✓		
Lian et al. (2017c)	✓		
Huang et al. (2021b)	✓		
Huang et al. (2022)	✓		
Vannoorenberghe et al. (1999)	✓	✓	
Bloch (1996)	✓	✓	
Taleb-Ahmed and Gautier (2002)	✓	✓	
Chaabane et al. (2009)	✓	✓	
Zhu et al. (2002)	✓	✓	
Bloch (2008)	✓	✓	
Chaabane et al. (2011)	✓	✓	
Ghasemi et al. (2012)	✓	✓	
Harrabi and Braiek (2012)	✓	✓	
Lelandais et al. (2012)	✓	✓	
Wang et al. (2013)	✓	✓	
Ghasemi et al. (2013)	✓	✓	
Lelandais et al. (2014)	✓	✓	
Makni et al. (2014)	✓	✓	
Derraz et al. (2015)	✓	✓	
Trabelsi et al. (2015)		✓	
Xiao et al. (2017)	✓	✓	
Lian et al. (2017a)	✓	✓	
Lian et al. (2018a)	✓	✓	
Tavakoli and Ghasemi (2018)	✓	✓	
Lima and Islam (2019)	✓	✓	
Lian et al. (2018b)	✓	✓	
Capelle et al. (2002)	✓		✓
Capelle et al. (2004)	✓		✓
Barhoumi et al. (2007)	✓		✓
Guan et al. (2011)	✓		✓
Ketout et al. (2012)	✓		✓
Wen et al. (2018)	✓		✓
George et al. (2020)	✓		✓
Huang et al. (2021c)	✓		✓
Gautier et al. (2000)	✓	✓	✓
Lajili et al. (2018)	✓	✓	✓
Bloch (1996)		✓	
Huang et al. (2021a)		✓	✓

modality and multi-modality inputs, and introduce them in Sections 4.1 and 4.2, respectively.

4.1. Single modality evidence fusion

Figure 7 shows the flowchart of single modality evidence fusion with a single classifier (we only take the classifier as an example in the rest of our paper to simplify the explanation). The segmentation process comprises three steps: masses calculation, feature-level mass fusion, and decision-making. The inputs of the flowchart are single modality medical images. At first, K mass functions can be obtained from the masses calculation step for each pixel. It models image information into K mass functions by summing the evidence of K different BBA methods, or K kinds of input features, or K nearest neighbors (Refer to Section 2.5.3 for more details), or K prototype centers (Refer to Section 2.5.4 for more information). Then Dempster’s rule is used to fuse the feature-level mass functions. Finally, decision-making is done to obtain the final segmentation results and output the segmented mask. The classifier here could be the intensity-based classification methods such as threshold intensity, the probabilistic-based methods such as SVM, or the fuzzy set-based methods such as FCM, etc. The BBA methods are various, therefore we introduce them in specific tasks in the following. The methods presented in this section focus on feature-level evidence fusion.

Suh et al. (1993) developed a knowledge-based endocardial and epicardial boundary detection and segmentation system with cardiac MR image sequences. Pixel and location information were mapped into mass functions by Shafer’s model (Shafer, 1976). The two source mass functions were fused by using Dempster’s rule. Experiments were applied to cardiac short-axis images and have obtained an excellent success rate ($> 90\%$). However, this work only focused on cardiac boundary detection and did not discuss the details of the heart. Vauclin et al. (2005) proposed a BFT-based lungs and spinal canal segmentation model. K-means clustering algorithm was first used to perform a pre-segmentation. Then a 3D filter exploits the results of the pre-segmentation to compute the membership degree from spatial neighbors using Shafer’s model. Segmentation results showed the credal partition permits to reduce connection risks between trachea and lung when they are very close and between the left and right lungs at the anterior or posterior junctions.

Gerig et al. (2000) presented a method for automatic segmentation and characterization of object changes in time series of 3D MR images. A set of

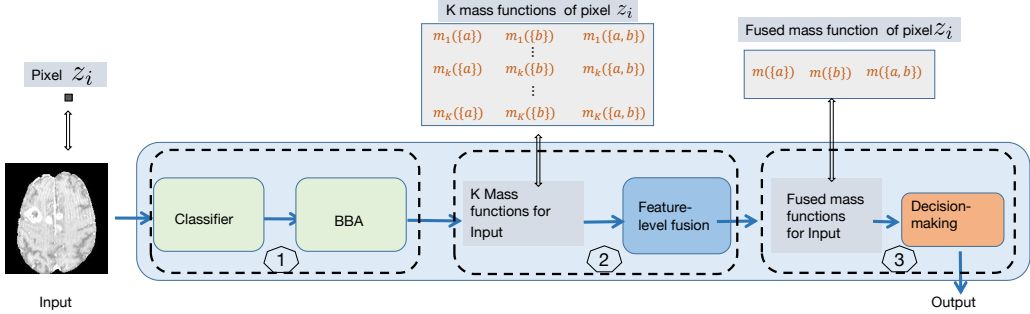


Figure 7: Example flowchart of single modality evidence fusion with single classifier. The segmentation process is composed of three steps: (1) image information are transferred into classifier/cluster and some BBA methods are used to get feature-level mass functions; (2) Dempster’s rule is used to fuse feature-level evidence; (3) decision-making is made based on the fused mass functions to output a segmented mask. We take only one pixel z_i as an example and show how BFT works on pixel-level evidence fusion under a binary segmentation task to simplify the process. For each pixel z_i , we can obtain K mass functions from BBA. After feature-level evidence fusion, a fused mass function is assigned to pixel z_i to represent the degree of belief this pixel belongs to class a, b and ignorance.

features was derived from time series according to brightness changes. BFOD transformation (Safranek et al., 1990) was used here to map the obtained features into mass functions. Then the set of evidence was combined by using Dempster’s rule. Experiments visually compared with results from alternative segmentation methods revealed an excellent sensitivity and specificity performance on the brain lesion region. The author also pointed out that better performance could be obtained with multi-modality and time-series evidence fusion. Simulation experimental results showed that about 80% of the implanted voxels could be detected for most generated lesions.

Vannoorenberghe and Flouzat (2006) presented a BFT-based thoracic image segmentation method. First, a K-means algorithm performed coarse segmentation on the original CT images. Second, the EKNN rule (Denœux, 1995) was applied by considering spatial information and calculate feature-level mass functions, which allows managing imprecise and uncertain data. The authors claimed that using the motioned segmentation scheme leads to a complementary approach combining region segmentation and edge detection. Experimental results showed promising results on 2D and 3D CT images for lung segmentation.

Derraz et al. (2013a) proposed an active contours (AC)-based (Chan et al., 2000) global segmentation method for vector-valued image that incorporated

both probability and mass functions. All features issued from the vector-valued image were integrated with inside/outside descriptors to drive the segmentation results by maximizing the Maximum-Likelihood distance between foreground and background. Appriou's second model (Appriou, 2005) was used to calculate the imprecision caused by low contrast and noise between inside and outside descriptors issued from the multiple channels. Then the fast algorithm based on Split Bregman (Goldstein and Osher, 2009) was used for final segmentation by forming a fast and accurate minimization algorithm for the Total Variation (TV) problem. Experiments were conducted on color biomedical images (eosinophil, lymphocyte, eosinophil, monocyte, and neutrophil cell (Mohamed and Far, 2012)) and have around 6% improvements by using F-score on five image groups. In the same year, (Derraz et al., 2013b) proposed a new segmentation method based on Active Contours (AC) for the vector-valued image that incorporates Bhattacharyya distance (Michailovich et al., 2007). The only difference is that the authors calculate the probability functions by Bhattacharyya distance in this paper instead of Maximum-Likelihood distance. The performance of the proposed algorithm was demonstrated on retinopathy dataset (Quellec et al., 2008; Niemeijer et al., 2009) and with an increase of 3% in F-score compared with the best-performed methods.

Lian et al. (2017b) introduced a tumor delineation method in fluorodeoxy glucose-positron emission tomography (FDG-PET) images by using spatial ECM (Lelandais et al., 2014) with adaptive distance metric. (Spatial ECM will be introduced in Section 4.2.3 because this method was proposed both for multi-modality evidence fusion). The authors proposed the adaptive distance metric to extract the most valuable features, and spatial ECM was used to calculate mass functions. Compared with ECM and spatial ECM, the proposed method showed a 14% and 10% increase in Dice score when evaluated on the FDG-PET images of non-small cell lung cancer (NSCLC) patients, showing good performance.

Huang et al. (2021b) proposed a 3D PET/CT lymphoma segmentation framework with BFT and deep learning. In this paper, as the PET and CT images were concatenated as two-channel input, we summarize this work as a signal modality input method in our review. The authors first transferred the concatenated 3D images into UNet to get high-level semantic features. Then the ENN classifier was used to map high-level semantic features into mass functions by fusing the contribution of K prototypes. Moreover, the segmentation uncertainty was considered in this paper with an uncertainty loss

during training. The reported quantitative and qualitative results showed that the proposal outperforms the state-of-the-art methods. Based on the first work, Huang et al. (2022) first compared the performance of RBF and ENN and then applied them within the deep neural network (UNet) for lymphoma segmentation. The segmentation performance confirmed that RBF is an alternative approach of ENN (Dencœux, 2019b) to act as an evidential classifier and showed that the proposal outperforms the baseline method UNet and the state-of-the-art.

4.2. *Multi-modality evidence fusion*

Single-modality medical images often do not contain enough information and are often tainted with uncertainty. That is why physicians always diagnose a disease with multiple sources of information, such as multi-MR images (native (T1), post-contrast T1-weighted (T1Gd), T2-weighted (T2), T2 Fluid Attenuated Inversion Recovery (FLAIR)) for brain tumor segmentation, or PET/CT images for lymphoma segmentation. In addition to feature-level (inner-modality) evidence fusion, the effective fusion of multi-modality (inter-modality) evidence is important in the medical domain for better disease diagnosis and radiotherapy. There are three main strains for the research of fusion strategies: probabilistic-based fusion, fuzzy set-based fusion, and BFT-based fusion. Thanks to developing deep learning and convolution neural networks (CNNs), researchers adopt probabilistic-based fusion methods on CNN and have achieved great success. Those probabilistic-based fusion methods can be summarised into three strategies (Zhou et al., 2019): image-level fusion (Wang et al., 2019; Isensee et al., 2017; Peiris et al., 2021) such as input data concatenation (Peiris et al., 2021), feature-level fusion (Dolz et al., 2018b,a; Zhou et al., 2020) such as attention mechanism concatenation (Zhou et al., 2020), and decision-level fusion such as averaging strategy (Kamnitsas et al., 2017; Nie et al., 2016) such as model ensembles (Kamnitsas et al., 2017). Though these methods have achieved good performances in some cases, the problem of the shortage of robust fusion remains, i.e., the ability to effectively manage conflicts that occur between different modalities and the explainable of the fused methods.

In this section, we introduce the BFT-based segmentation methods with multi-modality evidence fusion. Figure 8 shows an example flowchart of multi-modality evidence fusion with a single classifier. Compared with single modality evidence fusion, multi-modality evidence fusion focuses not only on feature-level but also on modality-level evidence fusion. The feature-level

evidence fusion is not necessary for this section. Multi-modality evidence fusion is the most popular application for BFT in the medical image segmentation domain. Therefore, we classify those methods according to their input modality for better analysis in this section.

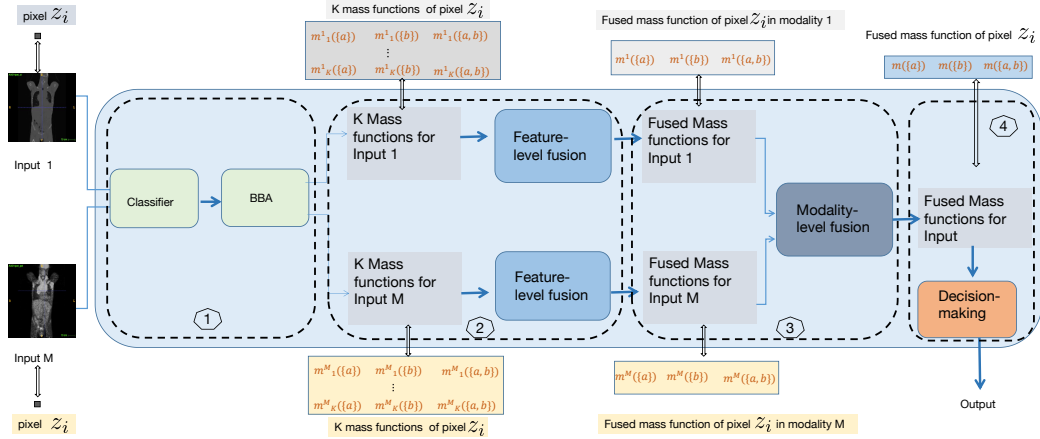


Figure 8: Example flowchart of multi-modality evidence fusion with a single classifier. The segmentation process is composed of four steps: (1) for each modality input, image features are fed into the classifier and some BBA methods are used to get feature-level mass functions; ((2) inside each modality, the calculated feature-level mass functions are fused by using Dempster’s rule to generate modality-level mass functions; (3) between the modalities, the calculated modality-level mass functions are fused by using Dempster’s rule again; (4) decision-making is made based on the fused mass functions to output a segmented mask. To simplify the introduction, we show the segmentation example of the same located pixels z_i^1 and z_i^M obtained from modality 1 and M . The same located pixel from different modalities are transferred separately into one classifier, and some BBA is used to get pixel-level mass functions. Similar to Figure 7, we assume for each pixel, we can obtain K mass functions. After feature-level and modality-level evidence fusion, a fused mass function is assigned to the pixel z_i to represent the degree of belief this pixel belongs to class a, b and ignorance.

4.2.1. Fusion of multi-modality MR images

Bloch (1996) pointed out some key features of BFT for data fusion by modeling uncertain and imprecision, introducing partial or global ignorance and fusing conflicting evidence. The way the author assigned mass functions in this paper is based on a reasoning approach that uses knowledge about the information (grey-level histograms) provided by each image to choose focal elements. After defining mass functions, then Dempster’s rule was used to

combine the mass from dual-echo MR images for each pixel. This paper is the first work that offered a full demonstration of the advantages of BFT on an example in images of pathological brains acquired with dual-echo MR images and have achieved good performance on brain tissue segmentation. Based on the first work with BFT, Bloch (2008) proposed to use fuzzy mathematical morphology (Bloch and Maître, 1995), i.e., erosion and dilation, for introducing imprecision in the mass functions and estimating compound hypotheses, then use Dempster’s rule to fuse multi-modality images under imprecision. The underlying assumption is that it is possible to represent imprecision by a set or a fuzzy set, which was called the structuring element in this paper. Application examples on dual-echo MR images fusion showed that the fuzzy mathematical morphology operations could represent either spatial domain imprecision or feature space imprecision (i.e., grey levels features). The visualized brain tissue segmentation results yield the robustness of the proposed method.

As we motioned in Section 2.6, Zhu et al. (2002) proposed modeling mass functions in BFT using fuzzy C-Means and spatial neighborhood information for image segmentation. The visualized segmentation results on MR brain images showed that the fusion-based segmented regions are relatively homogeneous, enabling accurate measurement of brain tissue volumes compared with single modality input MR image input.

Ghasemi et al. (2012) presented a brain tissue segmentation approach based on FCM and BFT. The authors used the FCM to model two different input features: pixel intensity and spatial information, as membership values (MVs). Then for each pixel, RMV transformation (Ghasemi et al., 2012) was used to map MVs into tissues. Last, the authors used Dempster’s rule to fuse intensity-based and spatial-based mass functions to get final segmentation results. Compared with FCM, the authors reported an increase in Dice and accuracy. As an extension of (Ghasemi et al., 2012), Ghasemi et al. (2013) proposed an unsupervised brain tumor segmentation method that modeled pixel intensity and spatial information into mass functions with RMV transformation and fused the two mass functions with Dempster’s rule.

Wang et al. (2013), proposed a lesion segmentation method for infarction and cytotoxic brain edema with BFT. The authors used a method similar to Zhu’s model to define simple and double hypotheses. FCM (Bezdek et al., 1984) was used first to construct the mass functions of simple hypotheses $\{a\}$ and $\{b\}$. Then the mass function of double hypotheses was defined by

$m(\{a, b\}) = \frac{1}{4} \times \frac{\min(m(\{a\}), m(\{b\}))}{m(\{a\}) + m(\{b\})}$. Then the authors used Dempster's rule for modality-level evidence fusion. The results showed that infarction and cytotoxic brain edema around the infarction could be well segmented by final segmentation. The qualitative one evaluated by two physicians showed that the proposed method could realize a good separation of cytotoxic brain edema and infarction.

Xiao et al. (2017) proposed an automatic vascular segmentation algorithm, which combines the grayscale and shape features of blood vessels and extracts 3D vascular structures from the head phase-contrast MR angiography dataset. First, grayscale and shape features are mapped into mass function by using the GD-based model. Second, a new reconstructed vascular image was established according to the fusion of vascular grayscale and shape features by Dempster's rule. Third, a segmentation ratio coefficient was proposed to control the segmentation result according to the noise distribution characteristic. Experiment results showed that vascular structures could be detected when both grayscale and shape features are robust. Compared with traditional grayscale feature-based and shape feature-based methods, the proposal showed better performance in segmentation accuracy with the decreased over-segmentation and under-segmentation ratios by fusing two sources of information.

Tavakoli and Ghasemi (2018) proposed a segmentation method based on the evidential fusion of different modalities (T1, T2, and Proton density (PD)) for brain tissue. The authors used FCM for initial segmentation and used the RMV transformation (Ghasemi et al., 2012) to transform the clustering membership value into mass functions by using RMV. The authors first formed the belief structure for each modality image and used Dempster's rule to fuse the three modalities' mass functions of T1, T2, and PD. Compared with FCM, this proposal achieved a 5% improvement in Dice score. Based on Tavakoli's method, Lima and Islam (2019) proposed a modified brain tissue segmentation method. The authors tested their method with four modality inputs: T1, T2, PD, and Flair. The reported results outperformed both baseline method FCM and Tavakoli's method with four modality evidence fusion.

4.2.2. Fusion of RGB channels

Vannoorenberghe et al. (1999) pointed out that taking R, G, and B channels as three independent information sources can be limited and weak for medical image tasks. This paper proposed a color image segmentation

method based on BFT. They calculated the degree of evidence by mapping R, G, B channel's intensity into mass functions using the Gaussian distribution information (similar to GD-based model (Chen et al., 2012)) and the discounting algorithm. Then three pieces of evidence were fused with Dempster's rule. The proposed segmentation method had been applied to biomedical images to detect skin cancer (melanoma). Experiments showed a significant part of the lesion is correctly extracted from the safe skin. The authors also pointed out that some regions correspond to pixels that cannot be classified either to the safe skin or the lesion because only the pixel-level feature is not enough for hard-example segmentation.

Chaabane et al. (2009) proposed a color medical image segmentation method based on fusion techniques. Compared to (Vannoorenberghe et al., 1999), the authors first modeled the probability of each region belongs an image by a Gaussian distribution, then used Appriou's second model to map probability into mass functions. Three color channel evidence are then combined by Dempster's rule. Compared with single-channel segmentation results, the fused results achieved a 10% increase in segmentation sensitivity. Chaabane et al. (2011) presented another BFT-based segmentation method of automatic determination of the mass functions of color biomedical image segmentation. First, possibilistic c-means (PCM) clustering (Bezdek, 2013) was used to R, G, B channels to do initial segmentation in the fuzzy domain and then maps the segmentation results into the mass functions of simple and double hypotheses with Zhu's model (Zhu et al., 2002). Then, based on the initial segmentation results, another mass function was calculated associated with each pixel and its neighboring pixels. Finally, the authors used Dempster's rule to fuse two kinds of mass functions for each pixel. Experimental segmentation results in cell images highlight the effectiveness of the proposed method. Compared with the FCM-based fusion method, the proposal increased by 15% in sensitivity segmentation.

Different from the method (Vannoorenberghe et al., 1999; Chaabane et al., 2009, 2011) that decompose color images into R, G, B channels, paper (Harrabi and Braiek, 2012) presented a color image segmentation method that represents the color image with 6 color spaces (RGB, HSV, YIQ, XYZ, LAB, LUV), to increase the information quality and to get an optimal segmented image through evidence fusion. The segmentation method is based on multi-level thresholding and data fusion techniques. This method aims at combining evidence from different color spaces. First, it identifies the most significant peaks of the histogram by multi-level thresholding with the two-

stage Otsu optimization approach. Second, the GD-based model was used to calculate the mass functions for each color space. Then the authors used Dempster’s rule to combine six sources of information. Compared with single color space, such as RGB and HSV, the fused result of six color spaces has a great increase in segmentation sensitivity, for example, an increase of 4% and 7% in RGB and HSV, respectively.

Trabelsi et al. (2015) applied BFT in optical imaging with color to improve skin lesion segmentation performance. The authors decomposed color images into R, G, B channels and applied the FCM method using the statistical features on each channel for probability assignment. After using FCM, three probability functions m_R , m_G and m_B can be obtained, corresponding to pixel x in three colors x_R , x_G and x_B . Then Dempster’s rule was applied to fuse the probability functions of the three channels to get the final segmentation results with equation $m_{R,G,B} = m_R \oplus m_G \oplus m_B$. Experiments showed about 10% improvement in segmentation accuracy compared with single-channel results. We should note that the authors only calculated the orthogonal sum of the probability functions for the three-channel images.

4.2.3. *Fusion of PET/CT*

Lelandais et al. (2012) proposed a BFT-based multi-trace PET images segmentation method to segment biological target volumes. First, the authors used a modified FCM algorithm with the discounting algorithm to determine the mass functions of voxels’ simple and complex hypotheses. The modification integrated a disjunctive combination of neighboring voxels inside the iterative process. Second, the operation of reduction of imperfect data was conducted by fusing neighboring voxels using Dempster’s rule. Based on this first work, Lelandais et al. (2014) proposed an ECM-based fusion model for biological target volumes segmentation with multi-tracer PET images. The authors first extended ECM with neighboring voxels information for modeling uncertainty and imprecision of mono-trace PET images. Then, the authors used prior knowledge related to defects in the acquisition system to reduce uncertainty and imprecision. Finally, the authors used Dempster’s rule for multi-tracer evidence fusion. Makni et al. (2014) introduced a similar work by using spatial neighborhood in ECM for multi-source image segmentation. The method achieved good performance on prostate multi-parametric MR images segmentation.

Derraz et al. (2015) proposed a framework to use both PET and CT images simultaneously for tumor segmentation. The authors proposed a Non-

Local Active Contours (NLAC) based variational segmentation framework to get probability results. Similar to (Derraz et al., 2013a,b), the authors used Appriou’s second model (Appriou, 2005) to calculate mass functions. Then the authors used Dempster’s rule to fuse the mass functions of PET and CT modality to achieve final segmentation results. The authors evaluated the proposed method on lung tumor segmentation to verify its effectiveness. Compared with the state-of-the-art method, this framework yielded the highest Dice score for tumor segmentation. Compared to manual contour delineations, this method is comparably high and has a small standard deviation.

Lian et al. (2017a) proposed a tumor segmentation method by using Spatial ECM (Lelandais et al., 2014) with Adaptive Distance Metric (Lian et al., 2017b) in FDG-PET images with the guidance of CT images. Lian et al. (2018b,a) proposed a co-segmentation method of lung tumor with PET/CT information modeling and fusion with BFT by considering that the two complementary imaging modalities can combine functional and anatomical information to improve segmentation performance. The authors adopted ECM to represent uncertain and imprecise image information. The authors adopted an adaptive distance metric for quantifying clustering distortions and spatial relationships during the evidential clustering procedure. Then the authors used Dempster’s rule to fuse the PET and CT segmentation results. The quantitative and qualitative evaluation results showed superior performance compared with single modality segmentation results with an increase of 1% and 58% in PET and CT in Dice score, respectively.

5. BFT-based medial image segmentation with several classifiers or clusterers

It is normal to see that two or more physicians cooperate for one patient’s disease diagnosis, which can minimize the impact of physicians’ misjudgments. Therefore, combining the results from multiple decision mechanisms and how to address their conflicts are of equal importance for a more reliable diagnosis. This section introduces the BFT-based medical image segmentation methods with several classifiers or clusters. We follow the same way in Section 4 to separate them into a single modality and multi-modality evidence fusion and introduce them in Section 5.1 and 5.2.

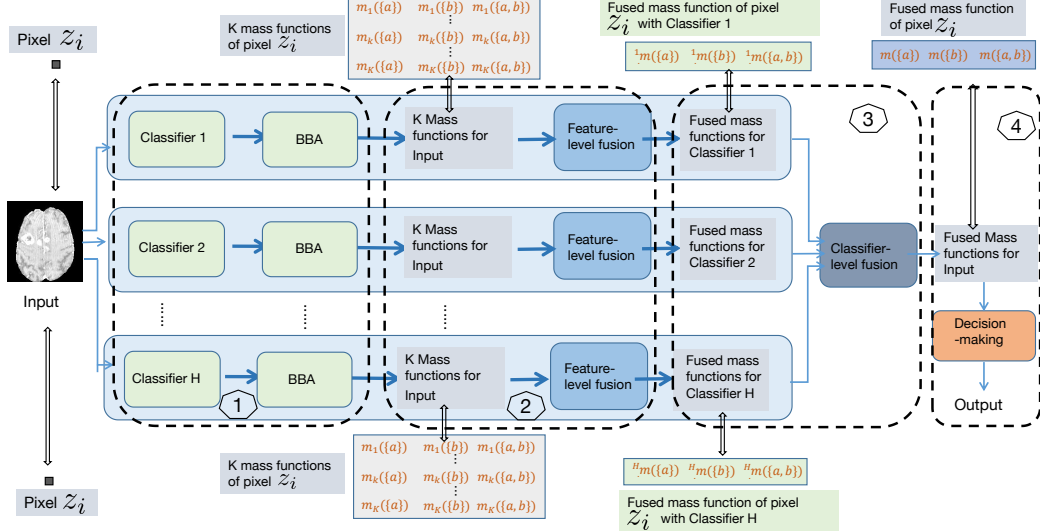


Figure 9: Example flowchart of single modality evidence fusion with several classifiers. The segmentation process is composed of four steps: (1) for each pixel, image features are transferred into different classifier, and some BBA methods are used to get feature-level mass functions; (2) inside each classifier, the calculated feature-level mass functions are fused by using Dempster’s rule to generate classifier-level mass functions; (3) between the classifiers, the calculated classifier-level mass functions are fused by using Dempster’s rule again; (4) decision-making is made based on the final fused mass functions and output a segmented mask. We take pixel z_i as an example. Similar to Figure 7, we assume for each pixel, we can obtain K mass functions by one classifier. After feature-level evidence fusion, for each pixel z_i , we can get H mass functions corresponding to H classifiers. Then we fuse the H mass functions and assign a fused mass function to the pixel z_i , representing the degree of belief this pixel belongs to class a, b and ignorance.

5.1. Single modality evidence fusion

Figure 9 shows an example flowchart of single modality evidence fusion with several classifiers. Different from the methods introduced in Section 4.1 that only have one classifier, several classifiers or clusters are used here. The results from multiple decision mechanisms can be regarded as the opinion of different physicians. The more classifiers or clusters we have, the more reliable decision we can get by reasonably aggregating those evidence. Compared with the methods presented in Section 4.1, the methods introduced in this section focus not only on feature-level but also on classifier-level evidence fusion to minimize the impact of misjudgments caused by the model’s inner shortcomings. The feature-level evidence fusion is not necessary for this section. We separate the segmentation process into four steps: mass

calculation, feature-level evidence fusion, classifier-level evidence fusion, and decision-making.

Capelle et al. (2002) proposed a segmentation scheme for MR images based on BFT. The authors followed the same idea of the Evidential K-NN rule (Denœux, 1995) to map image features into mass functions. Then, the authors applied the evidential fusion process to classify the voxels. Based on this first work, Capelle et al. (2004) proposed an evidential segmentation scheme of multi-modality MR images for brain tumors detection. This work focused on analyzing different evidential modeling techniques and on the influence of the introduction of spatial information to find the most effective brain tumor segmentation method. Three different BFT-based models: the distance-based BFT model (evidential K-NN) (Denœux, 2000), the likelihood function-based BFT method (Shafer's model (Shafer, 1976) and Appriou's first model ((Appriou, 1999)) were used to model information. Readers can refer to the sections in this paper where these methods have been recalled. The study concluded that neighborhood information increases the evidence of class membership for each voxel, thus making the final decision more reliable. Experimental results showed better segmentation performance compared with the state-of-the-art methods.

Taleb-Ahmed and Gautier (2002) proposed a segmentation method of MR sequences of vertebrae in the form of images of their multiple slices with BFT. The authors used three different classifiers to calculate three kinds of mass functions. Firstly, the authors used grey level intensity and standard deviation information to calculate two pixel-level mass functions with some fixed thresholds. Then the distance between two matching contours of consecutive slices (P and Q) to calculate contour-level mass functions with the following definition:

$$m(\{S_{PQ}\}) = 1 - e^{-\eta|d(P_i, Q_i) - \beta|}, \quad d(P_i, Q_i) \in [\rho.. \beta], \quad (38a)$$

$$m(\overline{\{S_{PQ}\}}) = 1 - e^{-\eta|d(P_i, Q_i) - \beta|}, \quad d(P_i, Q_i) \in [\beta.. \infty], \quad (38b)$$

$$m(\Omega) = e^{-\eta|d(P_i, Q_i) - \beta|}, \quad \forall d(P_i, Q_i), \quad (38c)$$

where P_i and Q_i are two matching points of the slices P and Q , $d(P_i, Q_i)$ is corresponding distance; $\Omega = \{S_{PQ}, \overline{S_{PQ}}\}$, S_{PQ} means two points P_i and Q_i are both belonging to cortical osseous. Parameter β represents the tolerance which the expert associates with the value $d(P_i, Q_i)$. Parameter ρ presents the inter-slice distance. The coefficient η makes it possible to tolerate a greater inaccuracy on the geometrical resemblance of two consecutive con-

tours. Then Dempster's rule was used to combine the above mass functions for final segmentation.

Barhoumi et al. (2007) introduced a new collaborative computer-aided diagnosis system for skin malignancy tracking. First, two diagnosis opinions were produced by perceptron neural network classification and content-based image retrieval (CBIR) schemes. Then Dempster's rule was used to fuse the two opinions to achieve a final malignancy segmentation. Simulation results showed that the proposed BFT-based combination could generate accurate diagnosis results. The frame of discernment in this paper is composed of the two singletons and the mas functions in this paper are said to be Bayesian.

Guan et al. (2011) proposed a human brain tissue segmentation method with BFT. The authors first used Markov random forest (MRF) (Li, 2009) for spatial information segmentation and then used a Two-Dimensional Histogram (TDH) method of fuzzy clustering (Duan and Guan, 2008) to get a vague segmentation. Then a redundancy image was generated, representing the difference between the MRF and TDH one. Then Zhu's model (Zhu et al., 2002) was used to calculate mass functions. Finally, Dempster's rule fused the two segmentation results and the generated redundancy image to handle controversial pixels. The visual segmentation results showed that this method has higher segmentation accuracy compared with the state-of-the-art methods.

As discussed in Section 3.2, Dempster's rule becomes numerically unstable when combining highly conflicting mass functions. In this condition, the fused results will be improper and any tiny changes of mass functions can bring sharp changes to the fusion results. Researchers in the medical domain has also awarded this limitation. Ketout et al. (2012) proposed a modified mass computation method to break this limitation and apply their proposal for endocardial contour detection. First, the output of each active contour model (ACM) (Kass et al., 1988) was regraded as mass functions. Second, a threshold was proposed to check if the evidence m conflicts with others. If there was conflict, a modifying operation was used on the conflicting evidence m : $m = m + 1/l$ with modified pace $1/l$. The parameter l is related to the number of hypothesis W in Ω , generally, $l = 2W$. Then the results of edge set-based segmentation (Li et al., 2005) and region set-based segmentation (Chan and Vese, 2001) were fused by using the improved BFT (Xin et al., 2005) to get a more accurate contour of the left ventricle. Experimental results showed that the fused contour is closer to the ground truth than the contour from the edge or region. And false detection of the two contours was

suppressed in the resulting image by rejecting the conflicting events by the fusion algorithm. Meanwhile, the proposed method could detect the edges of the endocardial borders even in low contrast regions.

Wen et al. (2018) proposed an improved MR images segmentation method based on FCM and BFT. First, the authors did a image-level fusion for two modality images A and B with the function $F(x, y) = w_1 \times g_A(x, y) + w_2 \times g_B(x, y)$, where x and y are image pixels and w_1 and w_2 are the weighted coefficients which are used to adjust the importance of different images for the final fusion result with $w_1 + w_2 = 1$. Second, the authors calculated the membership value by FCM and calculated the mass functions of simple and double hypotheses by Zhu’s model (Zhu et al., 2002) without the neighboring pixel information (refer to the section where this method is described in this paper). Third, the authors generated another mass function by weighting those of its neighboring pixels with the GD-based model and used Zhu’s model (Zhu et al., 2002) again to construct simple and double hypotheses mass functions. Finally, the authors used Dempster’s rule to complete the fusion of the two mass functions to achieve the final segmentation. Compared with the FCM-based method, the proposed method can better decrease the conflict in multiple sources to achieve easy convergence and significant improvement by using Dempster’s rule for classifier-level evidence fusion.

Besides, with the development of CNNs, the research community use Dempster’s rule for the fusion of multiple CNN classifiers. George et al. (2020) proposed a breast cancer detection system using transfer learning and BFT. This first work first applied BFT in multiple evidence fusion with deep learning. Image features were represented in high-level features using a convolutional neural network for feature extraction, such as ResNet-18, ResNet-50, ResNet-101, GoogleNet, and AlexNet. A patch-based feature extraction strategy was used to avoid wrong segmentation of the boundaries and provide features with good discriminative power for classification. The extracted features were classified into benign and malignant classes using a support vector machine (SVM). A discounting operation was applied to transfer probability-based segmentation maps into mass functions. The discounted outputs from the different CNN-SVM frameworks are now combined using Dempster’s rule. This work takes advantage of deep learning and BFT and has achieved good performance. Compared with majority voting-based fusion methods, BFT-based fusion showed superior segmentation accuracy. Compared with a single classifier, such as ResNet-101, the fused framework achieves the accuracy of sensitivity, specificity, specificity, and AUC with

an increase of 1%, 0.5%, 3%, and 2%, respectively. Also, the authors compared their results with the state-of-the-art method and achieved comparable segmentation accuracy.

Apart from using BFT just for evidence fusion, the more common way is to construct a belief framework directly. Huang et al. (2021c) proposed a BFT-based semi-supervised learning framework (EUNet) for brain tumor segmentation. This framework was constructed based on UNet and ENN. During training, two kinds of evidence were obtained: one is the segmentation probability maps generated directly by UNet and the other is the mass functions generated by EUNet. Dempster’s rule was used to fuse the two pieces of evidence. Experimental results showed that the proposal has better performance than state-of-the-art methods. It achieved around 10%, 4%, 2% increase in Dice score, Positive predictive value, and sensitivity, respectively, compared with the baseline (UNet). Moreover, the authors showed how BFT exceeds probability-based methods in addressing uncertainty boundary problems. Compared to (George et al., 2020) that uses BFT to fuse multiple CNN-based decisions, this work aims to embed BFT into CNN and achieves an end-to-end deep evidential segmentation model.

5.2. Multi-modality evidence fusion

The flowchart of multi-modality evidence fusion with multiple decision mechanisms is more complex than the flowchart we introduced in Sections 4.1, 4.2, and 5.1. The inputs of this flowchart are multi-modality medical images, and several classifiers or clusters are used. Figure 10 shows an example. The segmentation process comprises five steps: mass calculation, feature-level evidence fusion, classifier-level evidence fusion, modality-level evidence fusion, and decision-making. The feature-level evidence fusion is not necessary for this section. Pixels at the same position from different modalities are transferred into different classifiers and different BBA methods to get pixel-level mass functions. Dempster’s rule is used first to fuse feature-level evidence fusion, then to fuse classifier-level evidence, and last to fuse modality-level evidence.

Gautier et al. (2000) proposed a method for helping physicians to monitor the diseases of the spinal column with BFT. At first, an initial segmentation was applied with active contour (Lai, 1994) on multi-modality MR images. Then a frame of discernment was constructed according to experts’ opinions, and mass functions were obtained simultaneously. Thus, the mass functions here are human defined. Dempster’s rule was then used to fuse the mass

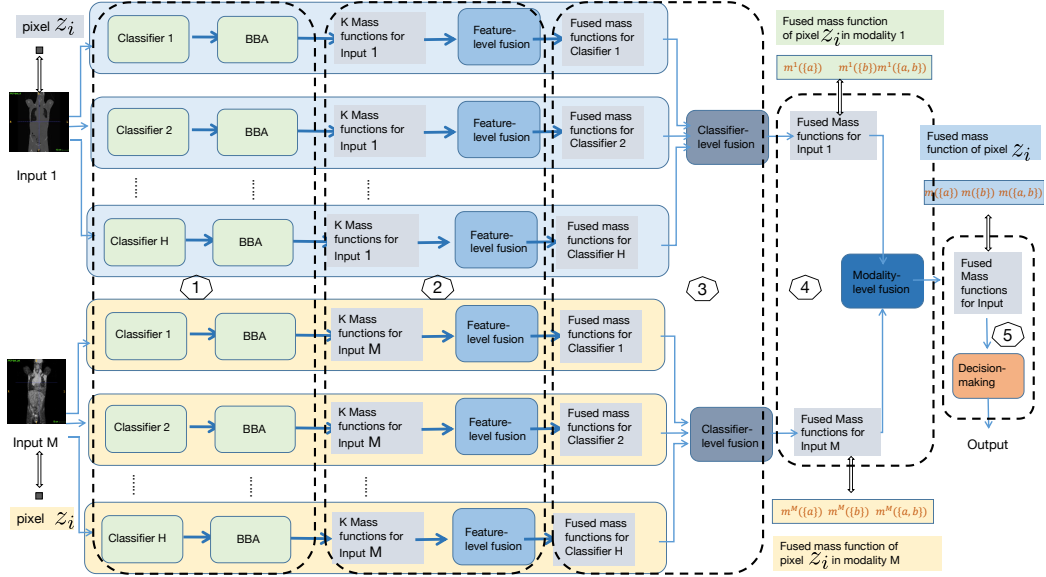


Figure 10: Example flowchart of multi-modality evidence fusion with several classifiers. The segmentation process is composed of five steps: (1) for each modality input, image features are fed into different classifiers and some BBA methods are used to get feature-level mass functions; (2) inside each classifier, the feature-level mass function are fused by Dempster’s rule to get classifier-level mass functions; (3) inside each classifier, the calculated classifier-level mass functions are fused by Dempster’s rule to get modality-level mass function; (4) inside each modality, the calculated modality-level mass functions are fused by Dempster’s rule; (5) decision-making is made based on the final fused mass functions and outputs a segmented mask. Here we show the segmentation example of the same located pixels z_i^1 and z_i^M that are obtained from modality 1 and M . The same pixel from different modalities is transferred separately into H classifiers and some BBA is used to get pixel-level mass functions. Similar to Figure 7, we assume for each pixel, we can obtain K mass functions with one classifier. After the fusion of feature-level, classifier-level and modality-level evidence fusion, a final mass function is assigned to the pixel z_i to represent the degree of belief this pixel belongs to class a, b and ignorance.

functions from different experts. Finally, the belief degree of contour points was obtained for segmentation decisions. The proposal got the most reliable segmentation maps with the experimental illustration results.

Lajili et al. (2018) proposed a two-step evidential fusion approach for breast region segmentation. The first evidential segmentation results were obtained by a grey-scale-based K-means clustering method. As the intensity of the grey-scale decreases from breast (Br) to background (Ba), the mass function of $m(\{Br\})$ also decreases and the value of $m(\{Ba\})$ increases. Sigmoid function was used to define the mass functions for each class $C_x (x = 1, \dots, k)$:

$$m_{z \in C_x}(\{Br\}) = \frac{1}{1 + \exp^{2-x}}, \quad (39a)$$

$$m_{z \in C_x}(\{Ba\}) = \frac{1}{1 + \exp^{-2-x}}, \quad (39b)$$

$$m_{z \in C_x}(\Omega) = 1 - m(\{Br\}) - m(\{Ba\}), \quad (39c)$$

where x denotes the index of the class C_x for pixel z . For local-homogeneity-based segmentation, the authors modeled the uncertainty with a threshold value α , by defining $m(\{Br\}) = 1 - \alpha$, $m(\{Ba\}) = 0$, $m(\{Br, Ba\}) = \alpha$, where α represents the belief mass affected by the uncertainty on the membership of the pixel z . A final fusion strategy with Dempster's rule was applied to combine evidence from two kinds of mass functions. Experiments were conducted on two breast datasets (Suckling, 1994; Bowyer et al., 1996). Compared with the best performed method, the proposed segmentation approach showed more accurate results. It extracted the breast region with correctness equal to 0.97, which is 9% higher than the best performed method.

Huang et al. (2021a), proposed to take PET and CT as two modality inputs and use to UNet model to segment lymphoma separately. Then the two obtained segmentation masks by Dempster's rule. Though this is the first work that applied BFT in multi-modality evidence fusion with several deep classifiers, the shortcoming of this work is that only probability functions other than mass functions are used for evidence fusion.

6. Conclusion and future work

6.1. Conclusion

The two main challenges we meet for medical image segmentation are poor medical image resolution and unreliable diagnosis ground truth, contrary to

high diagnosis and treatment requirements. Traditional machine learning-based medical image segmentation methods have limitations in uncertain information modeling and conflict information summarizing, which leads to poor segmentation accuracy. The application of deep neural networks has increased segmentation accuracy significantly more than traditional medical image segmentation methods by its powerful feature extraction and representation ability. Besides, researchers could apply more potential algorithms for medical image segmentation for helping clinical treatments.

This review paper provides a comprehensive overview of the BFT-based medical image segmentation methods, covering a range of existing BFT-based approaches for segmenting different human tissues (i.e., heart, lung) and tumors (i.e., brain, breast, and skin tumor). We analyzed these BFT-based medical image segmentation methods mainly through the way they model data and fuse evidence.

In particular, we first presented and discussed the history and the fundamental knowledge of BFT in Section 2. Then we gave an overall review and analysis of BFT-based medical image segmentation methods in Section 3. Sections 4 and 5 introduced detailed BFT-based medical image segmentation methods. Section 4 introduced the BFT-based medical image segmentation methods with a single classifier or cluster. Those methods use different methods to calculate mass functions and fuse them by Dempster’s rule. We separated the fusion operation mentioned in Section 4 into feature-level and modality-level evidence fusion according to the number of the input modality. Section 5 introduced the BFT-based medical image segmentation methods with several classifiers or clusters. Those methods use different methods to calculate mass functions for different classifiers. The computed mass functions in Section 5 were first combined in feature-level, then in classifier-level, and last in modality-level. Similar to Section 4, We separated the fusion operation mentioned in Section 5 according to the number of the input modality. In certain cases, the BFT-based methods could surpass the probability-based methods by modeling information more effectively (with uncertainty or ignorance quantification in focal sets) and fusing multiple evidence in different stages, i.e., feature-level, modality-level, and classifier-level evidence fusion.

6.2. Future work

Whereas, there remain some limitations of BFT. First, the fusion operation may fail if some source information is unreliable or there are significant

conflicts between source information. We should be careful of using Dempster’s rule when countering this situation. Discounting (Shafer, 1976) is an effective operation for multiple evidence fusion when counter with imperfect or unreliable evidence. For example, Huang et al. (2022) claimed that mass function m comes from each prototype could be seen as a discounted Bayesian mass function with a discount rate in ENN. Thus the most reliable mass functions can be obtained after fusing the evidence from different prototypes. Xu (2014) applied the discounting operation in multi-sensor fusion for scene understanding to guide the autonomous driving system and achieved significant detection accuracy. Similar to the autonomous driving task, the decision of segmentation and diagnosis in the medical domain should be cautious and reliable. Researchers in the medical have made some contributions to address the conflict between source information, such as the modified mass computation method (Ketout et al., 2012). At the same time, more contributions could be made to achieve the most reliable decision and to help the AI-based medical image diagnosis system applicable by taking reliability discounting into consideration.

Second, only a few works have considered both BFT and deep learning for medical image segmentation. Paper (Huang et al., 2021a) is the first work applying BFT for multi-modality evidence fusion with several deep classifiers. While only probability functions are fused in this paper, so it can not be regarded as a principle BFT-based multi-modality evidence fusion framework with several classifiers. Paper (George et al., 2020) is a successful application of Dempster’s rule for multi-modality image fusion with the discounted probability distribution. Paper (Huang et al., 2021c) is the work that proposed an end-to-end UNet-based evidential segmentation network. This work models information uncertainty with ENN and fuses two sources of evidence. One evidence comes from a probabilistic model, and the other comes from an evidential model. Paper (Huang et al., 2021b) and (Huang et al., 2022) confirmed the similarity of ENN and RBF when acting as an evidential classifier and applied both the two models within a deep neural network for lymphoma segmentation. We think more achievements could be obtained by cooperating BFT and popular deep medical image segmentation model, such as UNet, VNet (Milletari et al., 2016) and nnUNet (Isensee et al., 2018), in the future.

Third, acquiring big labeled training data is particularly challenging in the medical domain, which has become the bottleneck of learning-based approaches. Some contributions in BFT were proposed to address the short

of annotation problems, such as soft labels (Quost et al., 2017), Evidential Clustering (NN-EVCLUS)(Denœux, 2021b), EKNN based on contextual discounting with partially supervised learning (Denœux et al., 2019). Researchers could refer to those papers to get some idea to address the short on annotation problems in the medical domain.

We hope this review can provide an intuitive understanding of BFT-based techniques that have made significant contributions to medical image segmentation, especially for uncertain or imprecise medical image analysis and multi-modality evidence fusion. We hope this review can increase awareness of common challenges in this field, and call for future contributions. Some exploration directions might be interesting: (1)The exploration of multi-modality or cross-modality evidence fusion with discounting operation; (2) The exploration of soft-labels and partially supervised learning within deep neural networks; (3) Partial or set-valued classification (Ma and Denœux, 2021), which assigns instances to sets of classes and enable to reduce the probability of misclassification, could be an interesting research topic in medical domain; (4) Model calibration (Guo et al., 2017) with BFT is also an interesting research direction by quantifying both the accuracy and confidence of the model.

Acknowledgements

This work was supported by the China Scholarship Council (No. 201808331005). It was carried out in the framework of the Labex MS2T, which was funded by the French Government, through the program “Investments for the future” managed by the National Agency for Research (Reference ANR-11-IDEX-0004-02)

References

- Appriou, A., 1999. Multisensor signal processing in the framework of the theory of evidence. Application of mathematical signal processing techniques to mission systems 32.
- Appriou, A., 2005. 01-approche générique de la gestion de l'incertain dans les processus de fusion multisenseur. Traitement du signal .
- Bai, C., Huang, L., Pan, X., Zheng, J., Chen, S., 2018. Optimization of deep convolutional neural network for large scale image retrieval. Neurocomputing 303, 60–67.

Barhoumi, W., Dhahbi, S., Zagrouba, E., 2007. A collaborative system for pigmented skin lesions malignancy tracking, in: 2007 IEEE International Workshop on Imaging Systems and Techniques, IEEE, Cracovia, Poland. pp. 1–6.

Batenburg, K., J., Sijbers, J., 2009. Adaptive thresholding of tomograms by projection distance minimization. *Pattern Recognition* 42, 2297–2305.

Bezdek, J., 2013. Pattern recognition with fuzzy objective function algorithms. Springer Science & Business Media.

Bezdek, J.C., Ehrlich, R., Full, W., 1984. Fcm: The fuzzy c-means clustering algorithm. *Computers & Geosciences* 10, 191–203.

Bloch, I., 1996. Some aspects of Dempster-Shafer evidence theory for classification of multi-modality medical images taking partial volume effect into account. *Pattern Recognition Letters* 17, 905–919.

Bloch, I., 2008. Defining belief functions using mathematical morphology—application to image fusion under imprecision. *International journal of approximate reasoning* 48, 437–465.

Bloch, I., Maître, H., 1995. Fuzzy mathematical morphologies: a comparative study. *Pattern recognition* 28, 1341–1387.

Bowyer, K., Kopans, D., Kegelmeyer, W., Moore, R., Sallam, M., Chang, K., Woods, K., 1996. The digital database for screening mammography, in: Third international workshop on digital mammography, Mammography, Chicago. p. 27.

Capelle, A.S., Colot, O., Fernandez-Maloigne, C., 2002. Segmentation of multi-modality mr images by means of evidence theory for 3d reconstruction of brain tumors, in: Proceedings. International Conference on Image Processing, IEEE, New York, USA. pp. II–II.

Capelle, A.S., Colot, O., Fernandez-Maloigne, C., 2004. Evidential segmentation scheme of multi-echo mr images for the detection of brain tumors using neighborhood information. *Information Fusion* 5, 203–216.

Chaabane, S., Fnaiech, F., Sayadi, M., Brassart, E., 2009. Relevance of the Dempster-Shafer evidence theory for image segmentation, in: 3rd International Conference on Signals, Circuits and Systems (SCS), IEEE, Medenine, Tunisia. pp. 1–4.

Chaabane, S.B., Sayadi, M., Fnaiech, F., Brassart, E., Betin, F., 2011. A new method for the estimation of mass functions in the Dempster-Shafer's evidence theory: application to colour image segmentation. *Circuits, Systems, and Signal Processing* 30, 55–71.

Chan, T., Sandberg, B., Vese, L., 2000. Active contours without edges for vector-valued images. *Journal of Visual Communication and Image Representation* 11, 130–141.

Chan, T.F., Vese, L.A., 2001. Active contours without edges. *IEEE Transactions on image processing* 10, 266–277.

Chen, X., Zou, D., Zhao, Q., Tan, P., 2012. Manifold preserving edit propagation. *ACM Transactions on Graphics (TOG)* 31, 1–7.

Çiçek, Ö., Abdulkadir, A., Lienkamp, S.S., Brox, T., Ronneberger, O., 2016. 3D u-net: learning dense volumetric segmentation from sparse annotation, in: International conference on medical image computing and computer-assisted intervention, Springer, Athens, Greece. pp. 424–432.

Ciresan, D., Giusti, A., Gambardella, L.M., Schmidhuber, J., 2012. Deep neural networks segment neuronal membranes in electron microscopy images, in: Advances in Neural Information Processing Systems, Lake Tahoe, USA. pp. 2843–2851.

Dempster, A.P., 1967. Upper and lower probability inferences based on a sample from a finite univariate population. *Biometrika* 54, 515–528.

Denœux, T., 1995. A k-nearest neighbor classification rule based on Dempster-Shafer theory. *IEEE Transactions on Systems, Man, and Cybernetics* 25, 804–813. doi:10.1109/21.376493.

Denœux, T., 2000. A neural network classifier based on Dempster-Shafer theory. *IEEE Transactions on Systems, Man, and Cybernetics-Part A: Systems and Humans* 30, 131–150.

Denœux, T., 2008. Conjunctive and disjunctive combination of belief functions induced by nondistinct bodies of evidence. *Artificial Intelligence* 172, 234–264.

Denœux, T., 2011. Maximum likelihood estimation from uncertain data in the belief function framework. *IEEE Transactions on knowledge and data engineering* 25, 119–130.

Denœux, T., 2019a. Decision-making with belief functions: A review. *International Journal of Approximate Reasoning* 109, 87–110.

Denœux, T., 2019b. Logistic regression, neural networks and Dempster-Shafer theory: A new perspective. *Knowledge-Based Systems* 176, 54–67.

Denœux, T., 2021a. Nn-evclus: Neural network-based evidential clustering. *Information Sciences* 572, 297–330.

Denœux, T., 2021b. NN-EVCLUS: Neural network-based evidential clustering. *Information Sciences* 572, 297–330.

Denœux, T., 2022. Reasoning with fuzzy and uncertain evidence using epistemic random fuzzy sets: general framework and practical models. arXiv preprint arXiv:2202.08081 .

Denœux, T., Kanjanatarakul, O., 2016. Evidential clustering: a review, in: *International symposium on integrated uncertainty in knowledge modelling and decision making*, Springer, Cham. pp. 24–35.

Denœux, T., Kanjanatarakul, O., Sriboonchitta, S., 2019. A new evidential k-nearest neighbor rule based on contextual discounting with partially supervised learning. *International Journal of Approximate Reasoning* 113, 287–302.

Denœux, T., Masson, M., 2003. Clustering of proximity data using belief functions, in: *Intelligent systems for information processing*. Elsevier, pp. 291–302.

Denœux, T., Masson, M.H., 2004. Evclus: evidential clustering of proximity data. *IEEE Transactions on Systems, Man, and Cybernetics, Part B (Cybernetics)* 34, 95–109.

Derraz, F., Boussahla, M., Peyrodié, L., 2013a. Globally segmentation using active contours and belief function, in: International Conference on Advanced Concepts for Intelligent Vision Systems, Springer, Poznań, Poland. pp. 546–554.

Derraz, F., Pinti, A., Boussahla, M., Peyrodié, L., Toumi, H., 2013b. Image segmentation using active contours and evidential distance, in: Iberoamerican Congress on Pattern Recognition, Springer, Havana, Cuba. pp. 472–479.

Derraz, F., Pinti, A., Peyrodié, L., Bousahla, M., Toumi, H., 2015. Joint variational segmentation of ct/pet data using non-local active contours and belief functions. *Pattern Recognition and Image Analysis* 25, 407–412.

Dolz, J., Desrosiers, C., Ayed, I., 2018a. IVD-Net: Intervertebral disc localization and segmentation in MRI with a multi-modal unet, in: International Workshop and Challenge on Computational Methods and Clinical Applications for Spine Imaging, Springer, Cham. pp. 130–143.

Dolz, J., Gopinath, K., Yuan, J., Lombaert, H., Desrosiers, C., Ayed, I., 2018b. Hyperdense-net: a hyper-densely connected cnn for multi-modal image segmentation. *IEEE transactions on medical imaging* 38, 1116–1126.

Duan, R., Guan, Y.H., 2008. Multi-threshold value segmentation approach for medical images [j]. *Journal of Computer Applications* 28, 196–197.

Dubois, D., Prade, H., 1988. Representation and combination of uncertainty with belief functions and possibility measures. *Computational intelligence* 4, 244–264.

Dubois, D., Prade, H., 2012. Possibility theory: an approach to computerized processing of uncertainty. Springer Science & Business Media.

Dunn, J., 1973. A fuzzy relative of the isodata process and its use in detecting compact well-separated clusters. *Journal of Cybernetics* 3, 32–57. URL: <https://doi.org/10.1080/01969727308546046>, doi:10.1080/01969727308546046.

Gautier, L., Taleb-Ahmed, A., Rombaut, M., Postaire, J.G., Leclet, H., 2000. Belief function in low level data fusion: application in MRI images of vertebra, in: Proceedings of the Third International Conference on Information Fusion, IEEE, Paris, France. pp. TUC5–3.

George, K., Faziludeen, S., Sankaran, P., 2020. Breast cancer detection from biopsy images using nucleus guided transfer learning and belief based fusion. *Computers in Biology and Medicine* 124, 103954.

Gerig, G., Welti, D., Guttmann, C., R., Colchester, A., C., Székely, G., 2000. Exploring the discrimination power of the time domain for segmentation and characterization of active lesions in serial mr data. *Medical Image Analysis* 4, 31–42.

Ghasemi, J., Ghaderi, R., Mollaei, M.K., Hojjatoleslami, S., 2013. A novel fuzzy Dempster-Shafer inference system for brain mri segmentation. *Information Sciences* 223, 205–220.

Ghasemi, J., Mollaei, M.R.K., Ghaderi, R., Hojjatoleslami, A., 2012. Brain tissue segmentation based on spatial information fusion by Dempster-Shafer theory. *Journal of Zhejiang University SCIENCE C* 13, 520–533.

Ghesu, F., Georgescu, B., Mansoor, A., Yoo, Y., Gibson, E., Vishwanath, R., Balachandran, A., Balter, J., Cao, Y., Singh, R., 2021. Quantifying and leveraging predictive uncertainty for medical image assessment. *Medical Image Analysis* 68, 101855.

Goldstein, T., Osher, S., 2009. The split bregman method for l1-regularized problems. *SIAM journal on imaging sciences* 2, 323–343.

Goodfellow, I., Pouget-Abadie, J., Mirza, M., Xu, B., Warde-Farley, D., Ozair, S., Courville, A., Bengio, Y., 2014. Generative adversarial nets, in: *Advances in neural information processing systems*, Montréal, Canada. pp. 2672–2680.

Grady, L., Schwartz, E.L., 2006. Isoperimetric graph partitioning for image segmentation. *IEEE transactions on pattern analysis and machine intelligence* 28, 469–475.

Guan, S., Khan, A.A., Sikdar, S., Chitnis, P.V., 2019. Fully dense unet for 2-d sparse photoacoustic tomography artifact removal. *IEEE journal of biomedical and health informatics* 24, 568–576.

Guan, Y.H., Luo, Y., Yang, T., Qiu, L., Li, J., 2011. Study on the application of MRF and fuzzy clustering as well as the DS theory to image fusion segmentation of the human brain, in: 4th International Conference on Intelligent Networks and Intelligent Systems, IEEE, Washington, USA. pp. 57–60.

Guo, C., Pleiss, G., Sun, Y., Weinberger, K., 2017. On calibration of modern neural networks, in: International Conference on Machine Learning, PMLR. pp. 1321–1330.

Hariharan, B., Arbeláez, P., Girshick, R., Malik, J., 2015. Hypercolumns for object segmentation and fine-grained localization, in: Proceedings of the IEEE conference on computer vision and pattern recognition, Boston, USA. pp. 447–456.

Harrabi, R., Braiek, E.B., 2012. Color image segmentation using multi-level thresholding approach and data fusion techniques: application in the breast cancer cells images. *EURASIP Journal on Image and Video Processing* 2012, 11.

Huang, L., Bai, C., Lu, Y., Chen, S., Tian, Q., 2019. Adversarial learning for content-based image retrieval, in: 2019 IEEE Conference on Multimedia Information Processing and Retrieval, IEEE, San Jose, California, USA. pp. 97–102.

Huang, L., Denœux, T., Tonnelet, D., Decazes, P., Ruan, S., 2021a. Deep pet/ct fusion with dempster-shafer theory for lymphoma segmentation, in: International Workshop on Machine Learning in Medical Imaging, Springer. pp. 30–39.

Huang, L., Ruan, S., Decazes, P., Denœux, T., 2021b. Evidential segmentation of 3d pet/ct images, in: International Conference on Belief Functions, Springer. pp. 159–167.

Huang, L., Ruan, S., Decazes, P., Denœux, T., 2022. Lymphoma segmentation from 3d pet-ct images using a deep evidential network. *arXiv preprint arXiv:2201.13078* .

Huang, L., Ruan, S., Denœux, T., 2021c. Belief function-based semi-supervised learning for brain tumor segmentation, in: 2021 IEEE 18th International Symposium on Biomedical Imaging (ISBI), IEEE. pp. 160–164.

Huang, L., Ruan, S., Denœux, T., 2021d. Covid-19 classification with deep neural network and belief functions, in: The Fifth International Conference on Biological Information and Biomedical Engineering, Hangzhou, China. pp. 1–4.

Hurwicz, L., 1951. The generalized bayes minimax principle: a criterion for decision making under uncertainty. *Cowles Comm. Discuss. Paper Stat* 335, 1950.

Ibtehaz, N., Rahman, M.S., 2020. Multiresunet: Rethinking the u-net architecture for multimodal biomedical image segmentation. *Neural Networks* 121, 74–87.

Isensee, F., Kiefer, P., Wick, W., Bendszus, M., Maier-Hein, K.H., 2017. Brain tumor segmentation and radiomics survival prediction: Contribution to the brats 2017 challenge, in: International MICCAI Brainlesion Workshop, Springer, Cham. pp. 287–297.

Isensee, F., Petersen, J., Klein, J., Zimmerer, D., 2018. Nnu-net: Self-adapting framework for u-net-based medical image segmentation. *arXiv preprint arXiv:1809.10486* .

Jaffray, J., 1989. Linear utility theory for belief functions. *Operations Research Letters* 8, 107–112. URL: <https://www.sciencedirect.com/science/article/pii/0167637789900102>, doi:[https://doi.org/10.1016/0167-6377\(89\)90010-2](https://doi.org/10.1016/0167-6377(89)90010-2).

Kamnitsas, K., Bai, W., Ferrante, E., McDonagh, S., Sinclair, M., Pawlowski, N., Rajchl, M., Lee, M., Kainz, B., Rueckert, D., 2017. Ensembles of multiple models and architectures for robust brain tumour segmentation, in: International MICCAI Brainlesion Workshop, Springer, Cham. pp. 450–462.

Kass, M., Witkin, A., Terzopoulos, D., 1988. Snakes: Active contour models. *International journal of computer vision* 1, 321–331.

Ketout, H., Gu, J., Horne, G., 2012. Improved Dempster and Shafer theory to fuse region and edge based level set for endocardial contour detection, in: Proceedings of the 10th World Congress on Intelligent Control and Automation, IEEE, Beijing, China. pp. 5013–5018.

Kimmel, R., 2003. Fast edge integration, in: Geometric Level Set Methods in Imaging, Vision, and Graphics. Springer, New York, USA, pp. 59–77.

Kleinbaum, D., Hedeker, D., 1996. Logistic regression: a self-learning text. Statistical Methods in Medical Research 5, 103.

Krizhevsky, A., Sutskever, I., Hinton, G., 2012. Imagenet classification with deep convolutional neural networks, in: Advances in Neural Information Processing Systems, Lake Tahoe, USA. pp. 1097–1105.

Lai, K., 1994. Deformable contours: Modeling, extraction, detection and classification. Ph.D. thesis. University of Wisconsin–Madison.

Lajili, R., Kalti, K., Touil, A., Solaiman, B., Amara, N.E.B., 2018. Two-step evidential fusion approach for accurate breast region segmentation in mammograms. IET Image Processing 12, 1972–1982.

Lelandais, B., Gardin, I., Mouchard, L., Vera, P., Ruan, S., 2012. Segmentation of biological target volumes on multi-tracer pet images based on information fusion for achieving dose painting in radiotherapy, in: International Conference on Medical Image Computing and Computer-Assisted Intervention, Springer, Nice, France. pp. 545–552.

Lelandais, B., Ruan, S., Denceux, T., Vera, P., Gardin, I., 2014. Fusion of multi-tracer pet images for dose painting. Medical image analysis 18, 1247–1259.

Li, C., Xu, C., Gui, C., Fox, M.D., 2005. Level set evolution without re-initialization: a new variational formulation, in: IEEE computer society conference on computer vision and pattern recognition, IEEE, San Diego, California. pp. 430–436.

Li, S., 2009. Markov random field modeling in image analysis. Springer Science & Business Media.

Li, X., Yu, L., Chen, H., Fu, C.W., Heng, P.A., 2019. Transformation consistent self-ensembling model for semi-supervised medical image segmentation. *arXiv preprint arXiv:1903.00348* .

Lian, C., Li, H., Vera, P., Ruan, S., 2018a. Unsupervised co-segmentation of tumor in pet-ct images using belief functions based fusion, in: 2018 IEEE 15th International Symposium on Biomedical Imaging (ISBI 2018), IEEE, Washington, DC, USA. pp. 220–223.

Lian, C., Ruan, S., Denœux, T., Guo, Y., Vera, P., 2017a. Accurate tumor segmentation in fdg-pet images with guidance of complementary ct images, in: International Conference on Image Processing (ICIP), IEEE, Beijing, China. pp. 4447–4451.

Lian, C., Ruan, S., Denœux, T., Jardin, F., Vera, P., 2016. Selecting radiomic features from fdg-pet images for cancer treatment outcome prediction. *Medical image analysis* 32, 257–268.

Lian, C., Ruan, S., Denœux, T., Li, H., Vera, P., 2017b. Spatial evidential clustering with adaptive distance metric for tumor segmentation in fdg-pet images. *IEEE Transactions on Biomedical Engineering* 65, 21–30.

Lian, C., Ruan, S., Denœux, T., Li, H., Vera, P., 2017c. Tumor delineation in fdg-pet images using a new evidential clustering algorithm with spatial regularization and adaptive distance metric, in: 2017 IEEE 14th International Symposium on Biomedical Imaging (ISBI 2017), IEEE, Melbourne, Australia. pp. 1177–1180.

Lian, C., Ruan, S., Denœux, T., Li, H., Vera, P., 2018b. Joint tumor segmentation in pet-ct images using co-clustering and fusion based on belief functions. *IEEE Transactions on Image Processing* 28, 755–766.

Lima, S.A., Islam, M.R., 2019. A modified method for brain mri segmentation using Dempster-Shafer theory, in: 22nd International Conference on Computer and Information Technology, IEEE, Helsinki, Finland. pp. 1–6.

Long, J., Shelhamer, E., Darrell, T., 2015. Fully convolutional networks for semantic segmentation, in: Proceedings of the IEEE conference on computer vision and pattern recognition, Boston, USA. pp. 3431–3440.

Ma, L., Denœux, T., 2021. Partial classification in the belief function framework. *Knowledge-Based Systems* 214, 106742.

Makni, N., Betrouni, N., Colot, O., 2014. Introducing spatial neighbourhood in evidential c-means for segmentation of multi-source images: Application to prostate multi-parametric MRI. *Information Fusion* 19, 61–72.

Masson, M.H., Denœux, T., 2008. Ecm: An evidential version of the fuzzy c-means algorithm. *Pattern Recognition* 41, 1384–1397.

Masson, M.H., Denœux, T., 2009. Recm: Relational evidential c-means algorithm. *Pattern Recognition Letters* 30, 1015–1026.

Mercier, D., Quost, B., Denœux, T., 2008. Refined modeling of sensor reliability in the belief function framework using contextual discounting. *Information fusion* 9, 246–258.

Michailovich, O., Rathi, Y., Tannenbaum, A., 2007. Image segmentation using active contours driven by the bhattacharyya gradient flow. *IEEE Transactions on Image Processing* 16, 2787–2801.

Milletari, F., Navab, N., Ahmadi, S.A., 2016. V-net: Fully convolutional neural networks for volumetric medical image segmentation, in: 2016 fourth international conference on 3D vision, IEEE. pp. 565–571.

Mohamed, M., Far, B., 2012. An enhanced threshold based technique for white blood cells nuclei automatic segmentation, in: 14th International Conference on e-Health Networking, Applications and Services (Health-com), IEEE, Beijing, China. pp. 202–207.

Nie, D., Wang, L., Gao, Y., Shen, D., 2016. Fully convolutional networks for multi-modality isointense infant brain image segmentation, in: 2016 IEEE 13th international symposium on biomedical imaging (ISBI), IEEE, Prague, Czech Republic. pp. 1342–1345.

Niemeijer, M., Van Ginneken, B., Cree, M., Mizutani, A., Quellec, G., Sánchez, C., Zhang, B., Hornero, R., Lamard, M., Muramatsu, C., 2009. Retinopathy online challenge: automatic detection of microaneurysms in digital color fundus photographs. *IEEE transactions on medical imaging* 29, 185–195.

Nock, R., Nielsen, F., 2004. Statistical region merging. *IEEE Transactions on pattern analysis and machine intelligence* 26, 1452–1458.

Ohlander, R., Price, K., Reddy, D.R., 1978. Picture segmentation using a recursive region splitting method. *Computer Graphics and Image Processing* 8, 313–333.

Onoma, D., Ruan, S., Thureau, S., Nkhali, L., Modzelewski, R., Monnehan, G., Vera, P., Gardin, I., 2014. Segmentation of heterogeneous or small fdg pet positive tissue based on a 3d-locally adaptive random walk algorithm. *Computerized Medical Imaging and Graphics* 38, 753–763.

Peiris, H., Hayat, M., Chen, Z., Egan, G., Harandi, M., 2021. A volumetric transformer for accurate 3d tumor segmentation. *arXiv preprint arXiv:2111.13300* .

Peng, J., Estrada, G., Pedersoli, M., Desrosiers, C., 2020. Deep co-training for semi-supervised image segmentation. *Pattern Recognition* 107, 269. URL: <https://www.sciencedirect.com/science/article/pii/S0031320320300741>, doi:<https://doi.org/10.1016/j.patcog.2020.107269>.

Quellec, G., Lamard, M., Josselin, P., Cazuguel, G., Cochener, B., Roux, C., 2008. Optimal wavelet transform for the detection of microaneurysms in retina photographs. *IEEE transactions on medical imaging* 27, 1230–1241.

Quost, B., Denœux, T., Li, S., 2017. Parametric classification with soft labels using the evidential em algorithm: linear discriminant analysis versus logistic regression. *Advances in Data Analysis and Classification* 11, 659–690.

Ronneberger, O., Fischer, P., Brox, T.n., 2015. Convolutional networks for biomedical image segmentation, in: International Conference on Medical Image Computing and Computer-Assisted Intervention, Munich, Germany.

Ruan, S., Lebonvallet, S., Merabet, A., Constans, J.M., 2007. Tumor segmentation from a multispectral mri images by using support vector machine classification, in: 2007 4th IEEE International Symposium on Biomedical Imaging: From Nano to Macro, IEEE, Arlington, Virginia. pp. 1236–1239.

Safranek, R., Gottschlich, S., Kak, A., 1990. Evidence accumulation using binary frames of discernment for verification vision. *IEEE Transactions on Robotics and Automation* 6, 405–417.

Salvador, S., Chan, P., 2004. Determining the number of clusters/segments in hierarchical clustering/segmentation algorithms, in: 16th IEEE international conference on tools with artificial intelligence, IEEE, Boca Raton, USA. pp. 576–584.

Seyedhosseini, M., Sajjadi, M., Tasdizen, T., 2013. Image segmentation with cascaded hierarchical models and logistic disjunctive normal networks, in: Proceedings of the IEEE International Conference on Computer Vision, Sydney, Australia. pp. 2168–2175.

Shafer, G., 1976. A mathematical theory of evidence. Princeton university press.

Smets, P., 1990. The combination of evidence in the transferable belief model. *IEEE Transactions on pattern analysis and machine intelligence* 12, 447–458.

Strobl, C., Boulesteix, A.L., Zeileis, A., Hothorn, T., 2007. Bias in random forest variable importance measures: Illustrations, sources and a solution. *BMC bioinformatics* 8, 25.

Suckling, J., 1994. The mammographic image analysis society digital mammogram database. *Digital Mammo* , 375–386.

Suh, D., Eisner, R., Mersereau, R., Pettigrew, R., 1993. Knowledge-based system for boundary detection of four-dimensional cardiac magnetic resonance image sequences. *IEEE transactions on medical imaging* 12, 65–72.

Sun, L., Wang, Y., 2018. A multi-attribute fusion approach extending Dempster-Shafer theory for combinatorial-type evidences. *Expert Systems with Applications* 96, 218–229.

Suykens, J., Vandewalle, J., 1999. Least squares support vector machine classifiers. *Neural processing letters* 9, 293–300.

Taleb-Ahmed, A., Gautier, L., 2002. On information fusion to improve segmentation of mri sequences. *Information Fusion* 3, 103–117.

Tavakoli, F., Ghasemi, J., 2018. Brain mri segmentation by combining different mri modalities using Dempster-Shafer theory. *IET Image Processing* 12, 1322–1330.

Tong, Z., Xu, P., Denœux, T., 2021. An evidential classifier based on Dempster-Shafer theory and deep learning. *Neurocomputing* 450, 275–293.

Trabelsi, O., Tlig, L., Sayadi, M., Fnaiech, F., 2015. Skin lesion segmentation using the ds evidence theory based on the fcm using feature parameters, in: 12th International Multi-Conference on Systems, Signals & Devices (SSD15), IEEE, Sfax, Tunisia. pp. 1–5.

Vannoorenberghe, P., Colot, O., De Brucq, D., 1999. Dempster-Shafer's theory as an aid to color information processing. application to melanoma detection in dermatology, in: Proceedings 10th International Conference on Image Analysis and Processing, IEEE, Venice, Italy. pp. 774–779.

Vannoorenberghe, P., Flouzat, G., 2006. A belief-based pixel labeling strategy for medical and satellite image segmentation, in: 2006 IEEE International Conference on Fuzzy Systems, IEEE, Vancouver, BC, Canada. pp. 1093–1098.

Vauclin, S., Zhang, P., Gardin, I., O. Gallocher, O., Vannoorenberghe, P., 2005. Segmentation of thoracic computed tomography images, in: International Symposium on Signals, Circuits and Systems, Iasi, Romania. pp. 31–34. doi:10.1109/ISSCS.2005.1509843.

Velikova, M., Lucas, P.J., Samulski, M., Karssemeijer, N., 2012. A probabilistic framework for image information fusion with an application to mammographic analysis. *Medical Image Analysis* 16, 865–875.

Wang, L., Nie, D., Li, G., Puybareau, É., Dolz, J., Zhang, Q., Wang, F., Xia, J., Wu, Z., Chen, J.W., 2019. Benchmark on automatic six-month-old infant brain segmentation algorithms: the iseg-2017 challenge. *IEEE transactions on medical imaging* 38, 2219–2230.

Wang, R., Shen, X., Li, Y., Zhu, Y., Hui, C., Zhang, S., 2013. Lesion segmentation in acute cerebral infarction based on Dempster-Shafer theory, in: International Conference on Wavelet Analysis and Pattern Recognition, IEEE, Zurich, Switzerland. pp. 209–214.

Wen, J., Tian, Y., Yehang, S., Yongchuan, T., Weiwei, H., 2018. Improved evidential fuzzy c-means method. *Journal of Systems Engineering and Electronics* 29, 187–195.

Xiao, R., Ding, H., Zhai, F., Zhao, T., Zhou, W., Wang, G., 2017. Vascular segmentation of head phase-contrast magnetic resonance angiograms using grayscale and shape features. *Computer Methods and Programs in Biomedicine* 142, 157–166.

Xiao, X., Lian, S., Luo, Z., Li, S., 2018. Weighted res-unet for high-quality retina vessel segmentation, in: 9th International Conference on Information Technology in Medicine and Education (ITME), IEEE, Hangzhou, China. pp. 327–331.

Xin, G., Xiao, Y., You, H., 2005. An improved Dempster-Shafer algorithm for resolving the conflicting evidences. *International Journal of Information Technology* 11, 68–75.

Xu, P., 2014. Information fusion for scene understanding. Ph.D. thesis. Université de Technologie de Compiègne.

Yager, R., 1992. Decision making under Dempster-Shafer uncertainties. *International Journal of General System* 20, 233–245.

Yager, R., 2004. Decision making using minimization of regret. *International Journal of Approximate Reasoning* 36, 109–128. URL: <https://www.sciencedirect.com/science/article/pii/S0888613X03001270>, doi:<https://doi.org/10.1016/j.ijar.2003.10.003>.

Yager, R.R., 1987. On the Dempster-Shafer framework and new combination rules. *Information sciences* 41, 93–137.

Zhou, T., Canu, S., Ruan, S., 2020. Fusion based on attention mechanism and context constraint for multi-modal brain tumor segmentation. *Computerized Medical Imaging and Graphics* 86, 101811.

Zhou, T., Ruan, S., Canu, S., 2019. A review: Deep learning for medical image segmentation using multi-modality fusion. *Array* 3, 100004.

Zhu, W., Huang, Y., Tang, H., Qian, Z., Du, N., Fan, W., Xie, X., 2018. Anatomynet: Deep 3D squeeze-and-excitation u-nets for fast and fully automated whole-volume anatomical segmentation. *bioRxiv* , 392969.

Zhu, Y., Bentabet, L., Dupuis, O., Kaftandjian, V., Babot, D., Rombaut, M., 2002. Automatic determination of mass functions in Dempster-Shafer theory using fuzzy C-means and spatial neighborhood information for image segmentation. *Optical Engineering* 41, 760–770.

Zouhal, L.M., Deneux, T., 1998. An evidence-theoretic k-nn rule with parameter optimization. *IEEE Transactions on Systems, Man, and Cybernetics, Part C (Applications and Reviews)* 28, 263–271.